G65V Substitution in Actin Disturbs Polymerization Leading to Inhibited Cell Elongation in Cotton

Yongwang Sun[1,2], Wenhua Liang[1], Weijuan Shen[1], Hao Feng[1], Jiedan Chen[2], Zhanfeng Si[2], Yan Hu[2] and Tianzhen Zhang[1,2]*

[1] State Key Laboratory of Crop Genetics and Germplasm Enhancement, Cotton Hybrid R & D Engineering Center (the Ministry of Education), College of Agriculture, Nanjing Agricultural University, Nanjing, China, [2] Zhejiang Provincial Key Laboratory of Crop Genetic Resources, Institute of Crop Science, Plant Precision Breeding Academy, College of Agriculture and Biotechnology, Zhejiang University, Zhejiang, China

The importance of the actin cytoskeleton for proper cell development has been well established in a variety of organisms. Actin protein sequences are highly conserved, and each amino acid residue may be essential for its function. In this study, we report the isolation and characterization of $GhLi_1$ from an upland cotton mutant Ligon lintless-1 (Li_1), which harbors the G65V substitution in its encoded actin protein. Li_1 mutants exhibit pleiotropic malformed phenotypes, including dwarf plants, distorted organs, and extremely shortened fibers. Cytological analysis showed that the actin cytoskeleton was disorganized and the abundance of F-actin was decreased in the Li_1 cells. Vesicles were aggregated into patches, and excessive cellulose synthase complexes were inserted into the plasma membrane during the secondary cell wall biosynthesis stage, which dramatically affected the morphology of the Li_1 cells. Molecular model prediction suggested that the G65V substitution may affect the three-bodied G-actin interaction during F-actin assembly. Biochemical assays demonstrated that the recombinant $GhLi_1$ protein disturbs actin dynamics by inhibiting the nucleation and elongation processes. Therefore, our findings demonstrate that the G65V substitution in actin had dominant-negative effects on cell elongation, by disturbing actin polymerization and actin cytoskeleton-based biological processes such as intracellular transportation.

Keywords: actin polymerization, cell elongation, cotton, map-based cloning, plant morphology, short fiber

INTRODUCTION

The actin cytoskeleton is a fundamental and dynamic network in eukaryotic cells. It is not only involved in the maintenance of cell shape and structure, but also regulates a tremendous range of cellular processes, including cytoplasmic streaming, organelle movement, cell expansion, cell wall deposition and responses to internal and external signals (Staiger et al., 2000; Hussey et al., 2006). Actin exists in cells in a dynamic equilibrium between two principal forms: globular monomeric actin (G-actin) and filamentous polymeric actin (F-actin). Most of actin's biological functions are conducted by F-actin, which is assembled from G-actin subunits into a helical structure polymer (Holmes et al., 1990). A sophisticated regulatory system, represented by a plethora of actin binding proteins (ABPs), has developed to modulate actin dynamics, including assembly and disassembly of F-actins, and also their organization into higher-order networks (Blanchoin et al., 2010). The highly

dynamic and widely distributed actin cytoskeleton allows prompt responses of the cell to signals arising from developmental and environmental stimuli, ensuring the precise regulation of cell development (Staiger et al., 2000; Blanchoin et al., 2010).

Actin protein sequences vary little in length from 377 amino acid residues and share more than 80% protein sequence similarity (Šlajcherová et al., 2012). Amino acid substitutions in actin, especially those that have an impact on their surface properties, are very likely to alter actin-actin or actin-ABP interactions (McDowell et al., 1996; Feng and Marston, 2009). Numerous actin mutants caused by amino acid substitution have been found in both uni- and multi-cellular organisms. Some yeast actin mutations result in growth deficiencies, or even death of the cell (Ishiguro and Kobayashi, 1996; Teal and Dawson, 2007). In humans, many actin mutations have been found to be pathogenetic, and result in a range of congenital disorders, such as myopathy (Feng and Marston, 2009; Marston, 2018) and deafness (Bryan et al., 2006; Morin et al., 2009), depending on the site of mutation and the type of actin affected. In Arabidopsis, amino acid substitution in actin led to disruption of the F-actin network, resulting in various morphological malformations, such as dwarf plants and deformed organs (Ringli et al., 2002; Nishimura et al., 2003; Kato et al., 2010).

During plant cell growth, cell wall matrix precursors and membrane materials are constructed in the Golgi system, and then delivered to the existing cell wall at the site of expansion *via* exocytotic vesicles (Emons and Ketelaar, 2009). The membranes of these vesicles fuse with the plasma membrane (PM) causing the insertion of transmembrane proteins, typically represented by the cellulose microfibril-producing cellulose synthase complex (CSC), into the PM (Gardiner et al., 2003; Emons and Ketelaar, 2009). The importance of the actin cytoskeleton in plant cell growth had been well established by numerous pharmacological and genetic studies (Szymanski et al., 1999; Chen et al., 2009; Pei et al., 2012), and a growing body of evidence has confirmed that the actin cytoskeleton is essential in supporting the intracellular movement of cytoplasmic organelles (Miller et al., 1999; Mathur and Martin, 2002; Hussey et al., 2006; Akkerman et al., 2012). Any perturbation of the actin cytoskeleton by application of actin-depolymerizing drugs (Miller et al., 1999; Szymanski et al., 1999; Ketelaar et al., 2003; Chen et al., 2009), or spontaneous mutation or genetic manipulation of actin cytoskeleton related genes (Chen et al., 2002; Mathur and Martin, 2002; Nishimura et al., 2003; Wang et al., 2009; Kato et al., 2010; Yang et al., 2011; Zhang et al., 2011; Wu et al., 2015) affects cell elongation, expansion, and morphogenesis at various degrees. Accordingly, abnormal intracellular motility of organelles and vesicles has been observed, which directly results in altered cell morphogenesis (Wang et al., 2006; Gutierrez et al., 2009; Kato et al., 2010; Akkerman et al., 2012; Li et al., 2014).

Cotton is an important cash crop throughout the world, and its fibers are the primary raw material for the textile industry. The development of cotton fibers comprises four distinct, yet overlapping stages: fiber initiation, cell elongation, secondary cell wall (SCW) synthesis, and maturation (Haigler et al., 2012). There is a distinct rearrangement of the actin cytoskeleton during transition from fiber elongation to secondary wall deposition (Seagull, 1990; Wang et al., 2010). In line with the cytological

observations, a variety of ABP encoding genes have been found to be preferentially expressed in developing fiber cells, such as those encoding actin deploymerizing factors (Wang et al., 2009), profilins (Wang et al., 2005; Wang et al., 2010; Bao et al., 2011), and LIM-domain proteins (Han et al., 2013; Li et al., 2013; Li et al., 2018). Moreover, studies of transgenic cotton suggest that some increases in F-actin abundance are beneficial for fiber quality improvement (Wang et al., 2009; Han et al., 2013), and formation of the higher actin cytoskeleton structure plays a determinant role in the progression of developmental phases of cotton fibers (Wang et al., 2010; Zhang et al., 2017). However, the detailed physiological roles of the actin cytoskeleton in cell and plant morphogenesis remain poorly understood.

In *G. hirsutum*, Ligon lintless-1 (Li_1) is a monogenic dominant mutant that exhibits various abnormal morphological characteristics, including dwarf plants, twisted organs and extremely shortened fibers (Griffee and Ligon, 1929; Kohel, 1972). Therefore much work has been done to isolate the Li_1 gene (Karaca et al., 2002; Rong et al., 2005; Gilbert et al., 2013; Jiang et al., 2015; Thyssen et al., 2015). Recently, Thyssen et al. (2017) reported that the actin gene *Gh_D04G0865* is responsible for the Li_1 mutants. However, the molecular mechanisms underlying the action of the Li_1 gene are largely unknown. In this independent study, we isolated the same gene using a map-based cloning approach. Here, we named it *GhLi₁*, which harbors a missense mutation that causes the 65th glycine to be substituted with valine (G65V) in its gene product. Further analysis indicated that the G65V substitution in GhLi₁ affected the nucleation and elongation processes during the F-actin assembly, which disturbs actin cytoskeleton organization in a dominant manner. We also showed that GhLi₁ negatively regulates cotton plant morphology and fiber elongation by disordering the actin cytoskeleton-based processes such as intracellular transportation. Our results confirm and extend the current understanding of the role of the actin cytoskeleton in plant cell elongation.

MATERIALS AND METHODS

Plant Materials and Growth Conditions

The Li_1 mutants were provided by Dr. Kohel (USDA-ARS, College Station, TX, USA). It had been self-pollinated for at least six generations in our laboratory. Hai7124 is a commercial Sea-island *Verticillium*-resistant cultivar. Three BC₁ populations and two F₂ populations were developed from crosses between Li_1 and Hai7124 between 2011 and 2016 (**Supplementary Table S1**). Petals, ovules, and fibers were collected from the adult Li_1 mutants and wild-type (WT) plants. Roots, stems, and leaves were collected 15 days after germination (DAG) from seedlings grown in a growth chamber (16-h light/8-h dark, 28°C).

Measurement of the Length of Root Elongation Zone and Cells From This Zone in 7 DAG Seedlings

The length of root elongation zone was determined by measuring the distance between the bottom of mature zone (characterized

by root hairs) and the top of meristematic zone (V-shaped structure of apex) as described by Li et al. (2014). The length of cells from the root elongation zone was measured by the ImageJ software (https://imagej.nih.gov/ij/). Three-cm length root tips were incubated with FM4-64 staining buffer (5 mM) for 5 min at 25°C, and then observed under a LSM780 confocal laser microscope (Zeiss, Germany). The FM4-64 fluorescence was excited at 515 nm, with emission at 640 nm.

Scanning Electron Microscopy (SEM) Analysis

Cotyledons, ovules, and fibers were fixed with 2.5% glutaraldehyde in phosphate buffered saline (PBS, pH 7.0) for 24 h and washed three times with PBS for 15 min at each step. They were postfixed with 1% OsO_4 in PBS for 2 h, washed three times, then dehydrated by a graded series of ethano (30%, 50%, 70%, 80%, 90%, and 95%) for 15 min at each step, and finally dehydrated two times by absolute ethanol for 20 min. They were then coated with gold-palladium, and observed under a SEM (Hitachi Model SU-8010, Japan).

Transmission Electron Microscopy (TEM) Analysis

Fibers were detached from the mature seeds and pre-treated as described in SEM analysis. After pre-treatment, samples were subjected to absolute acetone for 20 min, 1:1 mixture of acetone and Spurr resin for 1 h at room temperature, 1:3 mixture of acetone and Spurr resin for 3 h and to final Spurr resin for 24 h, and embedded in Spurr resin to heat at 70°C for 9 h. Six-μm sections were generated, stained by uranyl acetate and alkaline lead citrate for 10 min, and finally viewed using a TEM (Hitachi Model H-7650, Japan).

Measurements of Length and Weight of Cotton Fibers

Bolls from the WT and Li_1 plants were harvested at 10–50 days post anthesis (DPA) at 10 day intervals. Seeds were separated from each other using a boiling method (Schubert et al., 1973). After washing in flowing water, the straightened fibers were measured using a vernier caliper. Fibers were then separated from seeds and fully dried, before being weighed on an analytical balance. Fiber density on each seed was calculated as the ratio of weight to length.

Determination of Cellulose Content in Cotton Fibers

Determination of the cellulose content in fibers was performed according to a method described previously (Zhang et al., 2017). Alcohol-insoluble fiber residues were treated with 2 M trifluoroacetic acid at 121°C for 90 min and centrifuged for 5 min. The pellets were re-suspended in 1-ml Updegraff reagent (acetic acid: nitric acid: water, 8:1:2) and incubated at 100°C for 30 min. After centrifugation, the residual materials were washed with water, 70% ethanol and acetone, in sequence, and then fully dried

and weighed. Cellulose content was calculated as a percentage of the weight of the residual materials to that of the initial samples.

Mapping of the Li_1 Gene

First, using three BC_1 populations and microsatellite markers that were developed based on genome sequences of G. raimondii (Paterson et al., 2012), the Li_1 locus was mapped to a 1.088-cm region on Chromosome D04 (Liang, 2015). To further delimit the mapping interval, we developed two F_2 populations and insertion-deletion (InDel) markers based on genome sequences of G. hirsutum and G. barbadense (Liu et al., 2015; Zhang et al., 2015). Finally, the Li_1 locus was delimited to a 630-kb interval on chromosome D04 of G. hirsutum. The cDNA and gDNA of 11 genes in this region were amplified from Li_1 and WT plants, and compared by Clustal X 2.0 software (Larkin et al., 2007). A single-nucleotide polymorphism (SNP) marker was developed according to the base mutation in Gh_D04G0865. Primer sequences used for mapping and gene cloning are listed in **Supplementary Table S2**. A SMARTer RACE cDNA amplification kit (Clontech, USA) was used to isolate the 5'- and 3'-untranslated regions (UTRs) of Gh_D04G0865.

Quantitative RT-PCR (qRT-PCR) Analysis

qRT-PCR analysis was performed on the ABI 7500 Real Time System (Applied Biosystems, USA). The amplification parameters were as follows: 95°C for 10 min, followed by 40 cycles at 95°C for 15 s, 58°C for 15 s, and 72°C for 15 s. The cotton Histone 3 gene (His3, GenBank accession no. AF024716) was used as the internal control. Amplification efficiency and gene specificity of qRT-PCR primers (**Supplementary Table S2**) were tested by Sanger sequencing and polyacrylamide gel electrophoresis.

Characterization of Actin Family Genes in G. hirsutum

The genomic database of G. hirsutum acc. TM-1 was downloaded from http://mascotton.njau.edu.cn/ (Zhang et al., 2015). Eight Arabidopsis actin protein sequences (McDowell et al., 1996) were used as queries to perform BLASTP search against the G. hirsutum protein sequence database. The identified actin genes were named as GhACTs based on their chromosomal location (**Supplementary Table S3**). ClustalX 2.0 software (Larkin et al., 2007) was used for the alignment of actin sequences from cotton and Arabidopsis. A phylogenetic tree was constructed by the Neighbor-Joining (NJ) method by MEGA v5.0 software and the reliability of interior branches was assessed with 1,000 bootstrap re-samplings (https://www.megasoftware.net/). The high-throughput RNA-sequencing data of G. hirsutum acc. TM-1 were employed from the accession code SRA: PRJNA248163 in the National Center for Biotechnology Information (https://www.ncbi.nlm.nih.gov/). Expression levels were calculated using the fragments per kilobase of exon model per million mapped reads (FPKM) method using Cufflinks software with default parameters (Trapnell et al., 2012). Heat map represent the spatio and temporal expression of GhACTs was drawing by Heml 1.0 software (Deng et al., 2014). Eight GhACTs were randomly

chosen for qRT-PCR experiment, and a correlation analysis was conducted to test the consistency in gene expression between qRT-PCR and RNA-Seq methods. Primers used for qRT-PCR are listed in **Supplementary Table S2**.

Virus Induced Gene Silencing (VIGS) Experiments in Cotton

Cotton VIGS assays were performed as described by Gao et al. (2011). Gene fragments were cloned into the pTRV2 vector and introduced into *Agrobacterium tumefaciens* strain GV3101. *Agrobacterium* cells were inoculated, harvested, and resuspended in infiltration medium (10-mM $MgCl_2$, 10-mM MES, 200-mM acetosyringone), and adjusted to an OD_{600} of 1.5. Cell suspensions were incubated at 25°C for 3 h, and then *Agrobacterium* cultures carrying pTRV1 and pTRV2 or its derivatives were mixed at a 1:1 ratio. WT and Li_1 seedlings (15 DAG) with fully expanded cotyledons and one true leaf were infiltrated by inserting the *Agrobacterium* suspension into the cotyledons. Primers used for vector construction and qRT-PCR analysis are listed in **Supplementary Table S2**.

Observation of the Actin Cytoskeleton in Fiber and Root Cells

Observation of the actin cytoskeleton in fiber cells was performed as described by Seagull (1990). Fibers were incubated in PBS buffer containing 100-mM PIPES, 0.05% Triton X-100, 1-mM $MgCl_2$, 3-mM DTT, 0.3-mM PMSF, 5-mM EGTA, 0.25% glutaraldehyde, and 0.66-μM AlexaFluor488-phalloidin for 10 min. The actin cytoskeleton in root cells was stained using the method described by Yang et al. (2011). Samples were incubated in PME buffer (100-mM PIPES, 5-mM $MgSO_4$, and 10-mM EGTA, pH 6.9) containing 300-μM MBS, 1.5% glycerol, and 0.1% Triton X-100 for 30 min. Samples were rinsed twice with PME buffer and then fixed in PME buffer containing 2% paraformaldehyde for 30 min. Samples were incubated in the staining buffer (PME, 1.5% glycerol, 0.1% Triton X-100, and 0.66-μM AlexaFluor488-phalloidin) at 4°C overnight, washed twice with PME and mounted onto glass slides. Observation of F-actin was performed under a LSM780 confocal laser microscope (Zeiss, Germany). AlexaFluor488 fluorescence was excited at 488 nm with emission at 543 nm.

Observation of Vesicles in Fiber and Root Cells

The distribution of vesicles in fiber and root cells was investigated according to the methods described by Zhao et al. (2010) and Li et al. (2014), respectively. Fibers and 1-cm root tips were respectively incubated with FM4-64 staining buffer (5 mM) for 10 min and 30 min at 25°C, and observed under a LSM780 confocal laser microscope (Zeiss, Germany). The FM4-64 fluorescence was excited at 515 nm, with emission at 640 nm.

Immunofluorescence Analysis of CSC Distribution in Fiber Cells

The distribution of CSC in fiber cells was investigated according to the method described by Wang et al. (2010). Twenty DPA fibers were fixed with 4% paraformaldehyde and 0.1% glutaraldehyde in PME buffer containing 0.1% Triton X-100 and 0.3 M mannitol. After three washes in PME buffer, fibers were incubated with 1% cellulase R-10 and 0.1% pectolase Y-23 in PME buffer for 5 min. Fibers were washed once in PME buffer and twice in PBS (pH 7.0), and further incubated in PBS containing 1% BSA for 15 min. The fibers were then probed with the primary antibody (anti-CesA7; Agrisera, Sweden) and the corresponding secondary antibody (AlexaFluor594-conjugated anti-rabbit IgG; Abbkine, USA), washed twice with PBS and observed. The AlexaFluor594 fluorescence was excited at 588 nm with emission at 612 nm.

Quantitative Analysis of Fluorescence Intensity

Quantification analysis of F-actin, vesicle, and CSC in fiber or root cells was conducted by ImageJ software (https://imagej. nih.gov/ij/) as described method by Zhang et al. (2011). Images belonging to the same comparison group were collected under the same condition, and then normalized to an equal grayscale. Sixty cells from six randomly selected visual fields were analyzed, and the region of interest size was 40 μm × 10 μm and 100 μm × 30 μm for fiber and root cell, respectively. The average pixel intensity were used to plot fluorescence intensity.

Molecular Model of G-Actin and F-Actin

The multiple alignment of 75 actin protein sequences (the 1–120 N terminal amino acids were presented) from yeast, Arabidopsis, rice, maize, poplar, and upland cotton was performed by Clustal X2.0 software. The accession number of these proteins are listed in **Supplementary Tables S4** and **S5**. The molecular model of G-actin was constructed using SWISS-MODEL software (https://www.swissmodel.expasy.org/) using a previously reported G-actin structure, 3chw.1.A, as the template. The polymer structure 6anu.1.E was used as the template to construct an F-actin model, and the Swiss-PdbViewer software was used to simulate the structural changes caused by the G65V substitution (Guex et al., 2009).

Recombinant Protein Production

The CDS of *GhLi₁* and *Ghli₁* were cloned into pET30a plasmids to construct *GhLi₁*-6×His and *Ghli₁*-6×His vectors, respectively. Recombinant proteins were expressed in *E. coli* strain BL21 (DE3) and purified using nickel-nitrilotriacetic acid resin. Purified GhLi₁-6×His and Ghli₁-6×His proteins were dissolved in Buffer A (5-mM Tris-HCl, pH 8.0, 0.2-mM $CaCl_2$, 0.2-mM ATP, 0.1-mM imidazole and 0.5-mM DTT) to generate Ca-ATP-actins.

Actin Nucleation Assay

Actin nucleation assays were conducted according to the methods described by Michelot et al. (2005). Mg-ATP-actin was prepared by incubation of Ca-ATP-actin with 1-mM EGTA and 0.1-mM $MgCl_2$ for 2 min on ice. Monomeric rabbit skeletal muscle actin (2 μM; 10% pyrene-labeled) was incubated with different concentrations of GhLi₁-6×His or Ghli₁-6×His for 5 min at room temperature. Pyrene fluorescence was detected by an F-4600

fluorescence spectrophotometer (Hitachi, Japan) immediately after the addition of one-tenth volume of 10×KMEI buffer (500-mM KCl, 10-mM MgCl$_2$, 10-mM EGTA, and 100-mM imidazole-HCl, pH 7.0). The fluorescence signal was detected every 50 s for a total of 20 min.

Fluorescence Microscopy of Actin Filaments *in Vitro*

In vitro actin filaments were observed as described previously (Michelot et al., 2005). Ghli$_1$-6×His and GhLi$_1$-6×His proteins were mixed at different concentrations (2:0, 2:0.2, 0:2, in a unit of "µM") in 1× KMEI buffer at 22°C for 5 or 20 min and labeled with an equimolar amount of rhodamine-phalloidin. The polymerized F-actin was diluted to 10 nM in fluorescence buffer (10-mM imidazole-HCl, pH 7.0, 50-mM KCl, 1-mM MgCl$_2$, 100-mM DTT, 100-µg/ml glucose oxidase, 15 mg/ml glucose, 20 µg/ml catalase, and 0.5% methylcellulose). A dilute sample of 2 µl was applied to a 22 × 22-mm cover slip coated with poly-L-Lys (0.01%). Actin filaments were observed with an Axio Imager D2 microscope (Zeiss, Germany) equipped with a 60×, 1.42-numerical aperture oil objective. Images were collected with a Axiocam 503 color camera using ZEN 2010 software. After 5-min polymerization, the number of actin filaments were calculated to reflect actin nucleation capacity. Ten 50 × 50-µm regions were randomly selected from the images to calculate the number of actin filaments. The data was finally normalized to number per 1 mm^2. After 20-min polymerization, the length of actin filaments were calculated to reflect actin elongation capacity. Ten 50 × 50-µm regions were randomly selected from the images to measure the length of actin filaments. The data represent means of each filament in each region. ImageJ software (https://imagej.nih.gov/ij/) were used in the measurement of filament number and length.

RESULTS

Li$_1$ Exhibits Defects in Cell Elongation

Compared with the WT, the Li$_1$ heterozygote showed reduced root growth and wrinkled cotyledons at the seedling stage (**Figure 1A** and **Table 1**), and dwarf plants, distorted stems, short internodes, wrinkled leaves, and petals (**Figures 1E–H**), and extremely shortened fibers at the later stages of development (**Figures 2A**, **B**). The Li$_1$ homozygote showed low survival rate and much weaker growth than the Li$_1$ heterozygote (**Figure 1E** and **Supplementary Table S1**). The more greatly affected phenotype of homozygote Li$_1$ than heterozygote indicates that
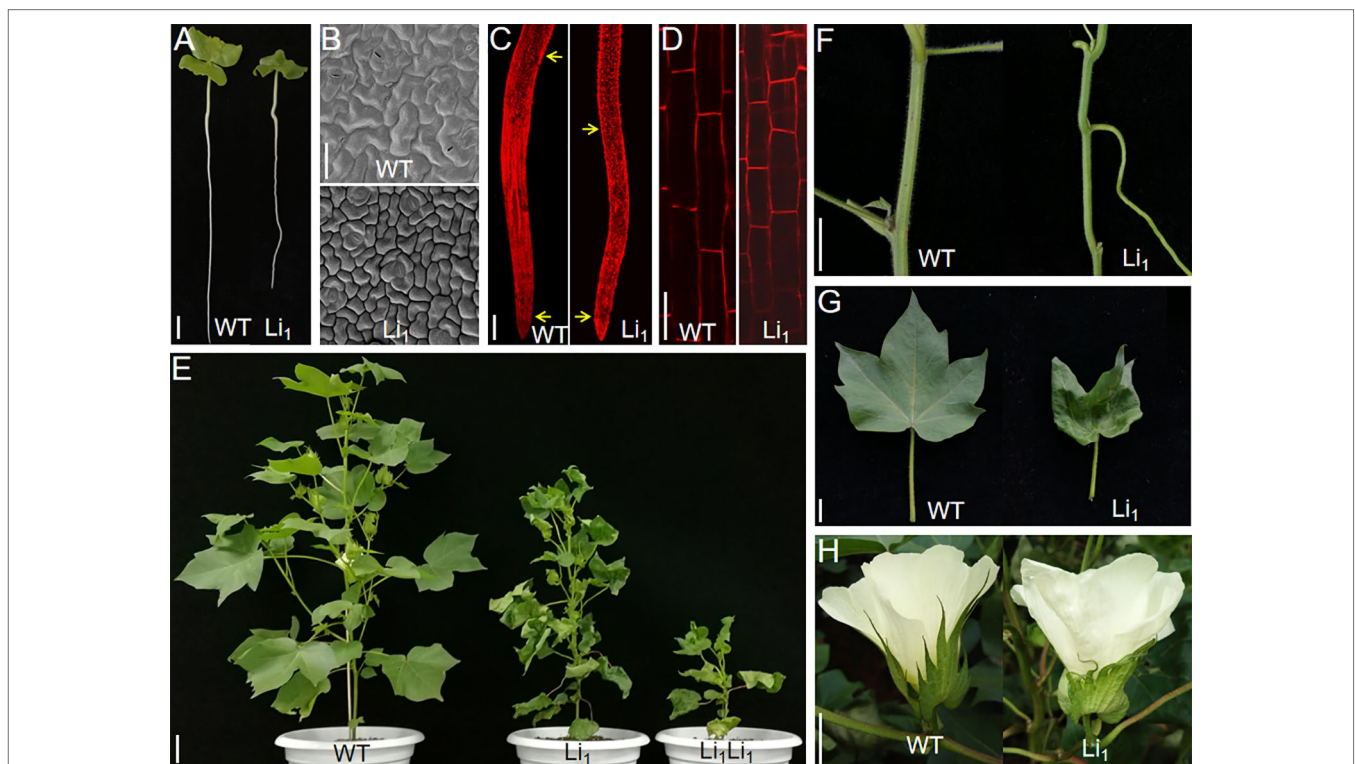
FIGURE 1 | Phenotypic differences between WT and Li$_1$. **(A)** WT and Li$_1$ seedlings (7 DAG), showing reduced root growth and wrinkled cotyledons in the Li$_1$. Bar = 2 cm. **(B)** SEM analysis of the cotyledon pavement cells of WT and Li$_1$ seedlings (7 DAG), showing reduced surface area of the pavement cells in the Li$_1$. Bar = 50 µm. **(C)** Root tips of WT and Li$_1$ seedlings (7 DAG). Arrows indicate borders of the root elongation zone (between the bottom of mature zone and the top of meristematic zone), showing shorter length of the root elongating zone in the Li$_1$. Bar = 0.1 cm. **(D)** Morphology of cortical cells in the root elongation zone of WT and Li$_1$, showing shorter cell length in the Li$_1$. Bar = 100 µm. **(E)** Compared with WT, the Li$_1$ heterozygote and homozygote (Li$_1$Li$_1$) mutants exhibited semi and extremely dwarf plants, respectively. Bar = 5 cm. **(F, G, H)** Stems **(F)**, leaves **(G)**, and calyxes and petals **(H)** of WT and Li$_1$ plants. Bars = 2 cm.

TABLE 1 | Comparison of phenotypic differences between WT and Li_1 seedlings (7 DAG).

Name	WT	Li_1
Length of the root	14.6 ± 1.8 cm	11.3 ± 1.3 cm**
Surface area of cotyledon pavement cells	1230 ± 151 µm²	462 ± 65 µm²**
Length of the root elongating zone	1.19 ± 0.16 cm	0.81 ± 0.11 cm**
Cell length in the root elongation zone	208.4 ± 23.1 µm	146.5 ± 14.0 µm**

*Data represent the means ± SD from 30 biological replicates. Student's t-test: **P < 0.01.*

the phenotypic differences are caused by a semi-dominant gene or a dosage effect, in line with our previous report (Liu et al., 2010). Since the Li_1 plants exhibited pleiotropic morphological changes, it is reasonable to speculate that the Li_1 gene is widely expressed in various organs/tissues. In addition, SEM analysis showed that the fiber development occurred at the same pace in the Li_1 and WT between 0 and 2 DPA, whereas the Li_1 fibers were obviously shorter than that of the WT on 3 DPA ovules (**Supplementary Figure S1**). Our observations are in agreement with those of previous studies (Karaca et al., 2002; Liang et al., 2015), suggesting that the Li_1 gene is not expressed until 3 DPA in developing fibers.

Given the smaller size of the Li_1 mutants, we sought to compare the cellular morphology of cotyledons and roots in Li_1 and WT plants. In the developing WT cotyledons, characteristic lobed and jigsaw-puzzle shaped pavement cells were found (**Figure 1B**). However, pavement cells in the Li_1 plants had fewer lobes, and their surface area was significantly reduced in comparison to the WT (**Figure 1B** and **Table 1**). In the WT, pavement cells maintained a firm contact with their neighbors, whereas contiguous epidermal cells in the Li_1 plants broke contact at their fringe, resulting in disconnected cells (**Figure 1B**). FM4-64 staining showed that the root elongation zone and cells from this zone were significantly shorter in Li_1 seedlings than that in WT (**Figures 1C, D** and **Table 1**). These results suggest that polar growth and elongation of the Li_1 cells was inhibited.

To gain more insights into the changes in developing Li_1 fiber cells, we determined the length and weight of the Li_1 and WT fibers at different developmental points. In the WT, fibers rapidly elongated between 10 and 20 DPA, and stopped at ~30 DPA. Whereas the elongation of Li_1 fibers nearly ceased at 10 DPA, and the Li_1 fibers were significantly shorter than the WT (**Figure 2C**). Although the dry weights of both Li_1 and WT fibers rapidly increased between 20 and 50 DPA (**Figure 2D**), the fiber density of Li_1 plants during this period was significantly higher than that of WT (**Figure 2E**). SEM analysis showed that the WT fibers adopt a flat ribbon like structure with a continuous helix, while the Li_1 fibers were shaped like circular tube and had no helix (**Figure 2F**). The increased density and altered shape of Li_1 fibers prompted us to investigate their cell wall structure. Cross-sections analysis showed the cell wall (especially the SCW) of mature Li_1 fibers had a much thicker appearance than that of the WT (**Figures 2G, H**). Statistical analysis showed that the thickness of the cell wall was
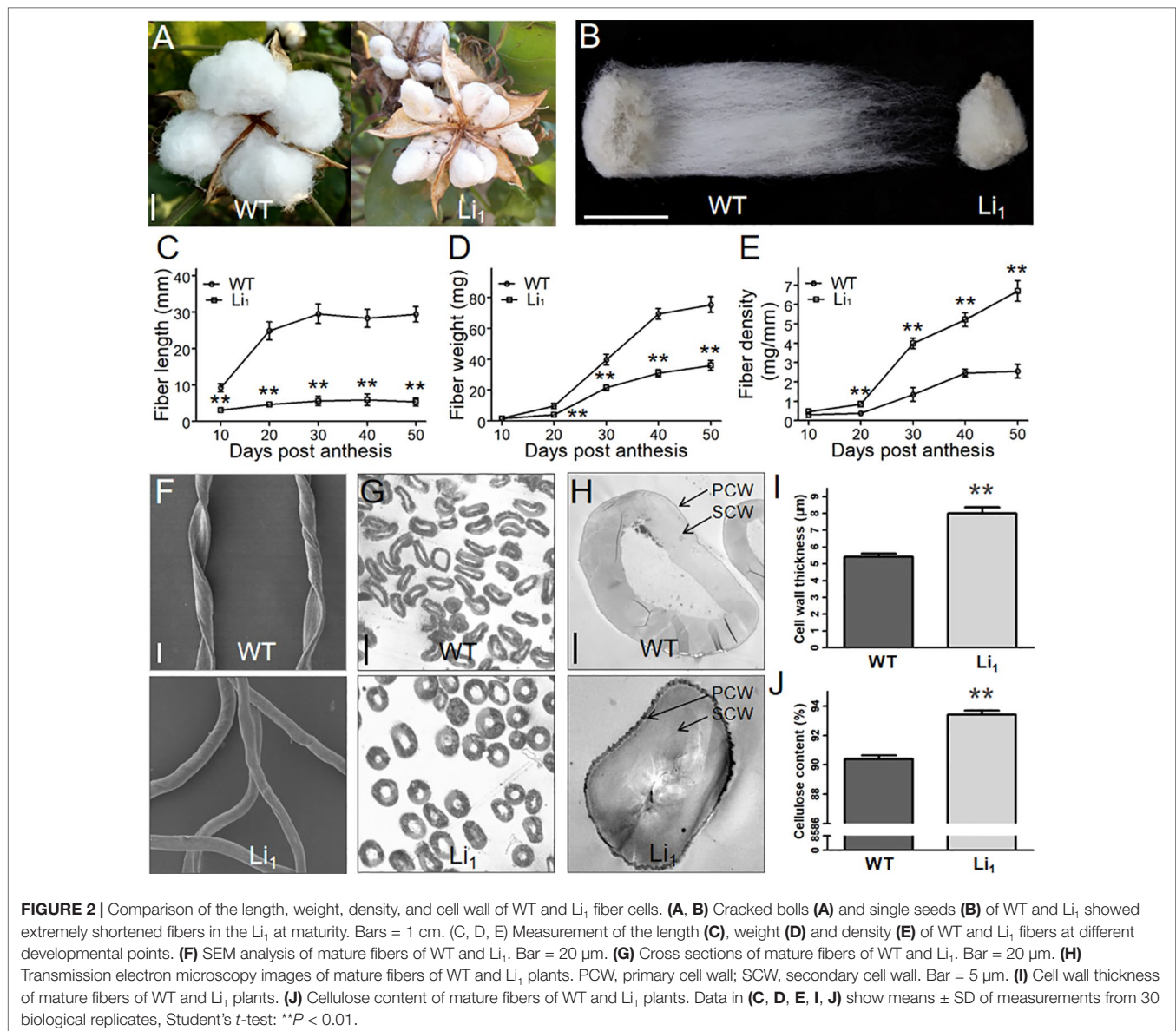
significantly higher in the Li_1 fiber cells (**Figure 2I**). Since the major component of mature cotton fiber cells is a SCW mainly consists of cellulose, the cellulose content of the mature fiber cells was measured. As shown in **Figure 2J**, the cellulose content of the Li_1 mature fibers was significantly higher than that of the WT. Thus, more active cellulose synthesis may account for the thicker SCW, increased fiber density and non-helical fiber cell shape of the mutants.

Mapping of the Li_1 Gene

To understand the mechanisms of Li_1 gene response to Li_1 mutant phenotype, we isolated the causative gene using a map-based cloning approach. The Li_1 locus was first mapped on chromosome D04 between the microsatellite markers W4806 and W4571 using three BC₁ populations, covering a 3.1 Mb interval (22.56–25.66 Mb) on chromosome D04 based on the genome sequence of *G. hirsutum* (**Figure 3A**; Liang, 2015; Zhang et al., 2015). Using two F₂ populations and InDel markers, the Li_1 locus was further narrowed down to a region between L408 and L440, covering a 630-kb interval that covering 11 annotated genes (**Figures 3B, C** and **Supplementary Table S3**) according to the *G. hirsutum* genome (Zhang et al., 2015). Sequence analysis showed that the 194th base of *Gh_D04G0865* had changing from "G" to "T" in the Li_1, resulting in the 65th amino acid residue being changed from glycine to valine (G65V) in the encoded actin (**Figure 3D**). Whereas the other ten genes had no sequence variation between the WT and Li_1. The SNP marker designed by the base mutation in the CDS of *Gh_D04G0865* was found to be co-segregated with the Li_1 phenotype (**Figure 3B**). The expression of annotated genes in the mapping region was determined in various organs and developing ovules (0, 3, 5 DPA) and fibers (10 DPA) from the WT and Li_1 plants (**Supplementary Figure S2**). Eight genes didn't conform to the broad spectrum expression feature of the Li_1 gene: *Gh_D04G0861*, *Gh_D04G0867*, *Gh_D04G0868*, and *Gh_D04G0869* did not express in all tested tissues; both *Gh_D04G0859* and *Gh_D04G0866* not in petals; *Gh_D04G0860* and *Gh_D04G0862* not in roots and petals, respectively. These genes didn't conform to the broad spectrum expression feature of the Li_1 gene, so they were excluded from candidate genes. The expression level of *Gh_D04G0863* and *Gh_D04G0864* could not be distinguished due to their sequence similarity, and they expressed in all the tested tissues. The expression of *Gh_D04G0865* could be found in all tissues except for the 0 DPA ovules. Statistical analysis showed the expression level of these genes were not significantly changed in Li_1 tissues in comparison to that in WT. However, interestingly, spatiotemporal expression pattern of *Gh_D04G0865* is highly consistent with the phenotypic features of Li_1, including the mutant phenotype in various tissues and the onset time (3 DPA) of abnormal development in fibers (**Figure 1** and **Supplementary Figures S1** and **S2**). Therefore, it was supposed that the actin gene *Gh_D04G0865* was the most likely candidate gene underlying the Li_1 locus.

Actin Family Genes in *G. hirsutum*

In higher plants, actin is typically encoded by a multigene family, and one of the most important feature of actin genes

FIGURE 2 | Comparison of the length, weight, density, and cell wall of WT and Li$_1$ fiber cells. **(A, B)** Cracked bolls **(A)** and single seeds **(B)** of WT and Li$_1$ showed extremely shortened fibers in the Li$_1$ at maturity. Bars = 1 cm. (C, D, E) Measurement of the length **(C)**, weight **(D)** and density **(E)** of WT and Li$_1$ fibers at different developmental points. **(F)** SEM analysis of mature fibers of WT and Li$_1$. Bar = 20 μm. **(G)** Cross sections of mature fibers of WT and Li$_1$. Bar = 20 μm. **(H)** Transmission electron microscopy images of mature fibers of WT and Li$_1$ plants. PCW, primary cell wall; SCW, secondary cell wall. Bar = 5 μm. **(I)** Cell wall thickness of mature fibers of WT and Li$_1$ plants. **(J)** Cellulose content of mature fibers of WT and Li$_1$ plants. Data in **(C, D, E, I, J)** show means ± SD of measurements from 30 biological replicates, Student's t-test: $**P < 0.01$.

is that they share high sequence similarity (Šlajcherová et al., 2012). Hence, understanding of the members, sequence characters, and expression patterns of the actin family genes in *G. hirsutum* is essential prior to the functional studies of *Gh_D04G0865*. A BLASTP search against the *G. hirsutum* genome identified 37 actin genes that dispersed on 20 of the 26 chromosomes. They were named as *GhACT1A~GhACT17A* and *GhACT1D~GhACT17D* according to their chromosomal location (**Supplementary Figure S3** and **Supplementary Table S4**). Arabidopsis actin family genes were the most thoroughly studied actin family genes in higher plants, they were grouped into vegetative and reproductive classes based on their phylogenetic relationship and expression pattern (McDowell et al., 1996). Phylogenetic analysis showed cotton actin genes were also divided into two classes A and B that clustered together with the reproductive and vegetative Arabidopsis actin genes,

respectively (**Supplementary Figure S4**). Subsequent divergence divided class A and B into three and two subclasses, respectively. Gene and protein sequence similarity of *GhACTs* with each other were higher than 80.17% and 90.64%, respectively. *Gh_D04G0865* (named as *GhACT9D* in this nomenclature) shares higher than 81.74% CDS similarity with other *GhACTs* (**Supplementary Figure S5**). Transcriptomic data showed the expression pattern of *GhACTs* were in concordance with their phylogenetic divergence. With a few exceptions, most *GhACTs* in the group A were specially expressed in the reproductive organs such as stamens and developing ovules, while most *GhACTs* in the group B were expressed in almost all organs (**Supplementary Figure S6**). Eight *GhACTs* were randomly selected for qRT-PCR analysis, and their relative expression level were highly correlated with the transcriptomic data, indicating both of the two methods were credible in detection of gene expression level
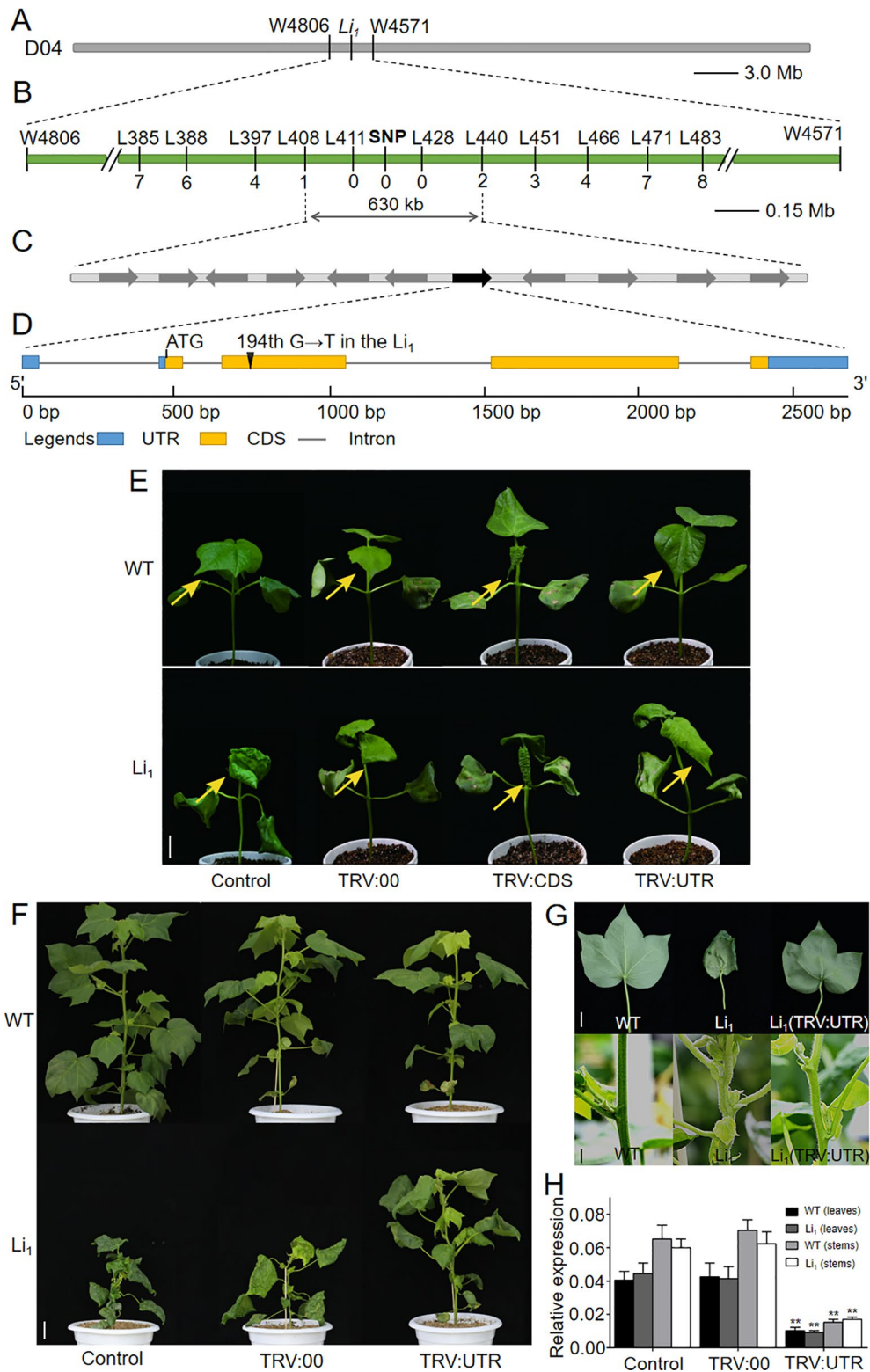
FIGURE 3 | Continued

FIGURE 3 | Map-based cloning and functional verification of the *Li₁* gene. **(A)** The *Li₁* locus was first mapped on chromosome D04 between the microsatellite markers W4806 and W4571 using three BC_1 populations. **(B)** The *Li₁* locus was further fine-mapped to a region between InDel markers L408 and L440 using two F_2 populations, and a SNP marker designed by the base mutation in *Gh_D04G0865* was found to be co-segregated with the mutant phenotype. **(C)** The 630-kb mapping region includes eleven annotated genes, among which *Gh_D04G0865* (indicated by green box) was the candidate gene responsible for the Li₁ mutants. **(D)** Gene structure of *Gh_D04G0865*. In the Li₁, the 194th base of *Gh_D04G0865* had changed from "G" to "T", resulting in the 65th amino acid residue being changed from glycine to valine (G65V) in the encoded actin. **(E)** Phenotypic changes were observed in the second true leaves (arrows indicated) 15 days after VIGS treatment. Bar = 2 cm. **(F)** The phenotypes of untreated (control), and pTRV2 (TRV:00) and pTRV2::UTR (TRV : UTR) treated WT and Li₁ adult plants (90 day after VIGS treatment). Bar = 5 cm. **(G)** Phenotype of the leaves and stems of WT, Li₁, and pTRV2::UTR treated Li₁ plants. Bars = 2 cm. **(H)** Expression level of *Gh_D04G0865* in leaves and stems in control, and TRV:00 and TRV : UTR treated WT and Li₁ adult plants. Data in **(H)** represent the means ± SD of three biological replicates, Student's *t*-test: **P < 0.01.

(**Supplementary Figure S7**). Expression pattern of *GhACTs* indicated that many members were likely to be simultaneously expressed in the given organs/tissues, and each gene product has the potential to participate in actin assembly to form hetero-polymer F-actins (Meagher et al., 1999).

Functional Verification of the *Li₁* Gene

Recently, Thyssen et al. (2017) reported that *Gh_D04G0865*, the same gene as we isolated, is responsible for the Li₁ mutants. To verify that this gene is the causal gene for *Li₁*, these researchers constructed a pTRV2 vector comprising its 781–1134-bp CDS (shares higher than 81.59% sequence similarity with other *GhACTs*) and 127 bp 3'-UTR, and VIGS experiments were performed in WT plants. The resultant decreased expression of *Gh_D04G0865* and the abnormal phenotypes of VIGS treated plants suggested that this gene is responsible for the Li₁ mutants. However, we have different opinions on the design of this experiment. Firstly, the VIGS vector constructed by Thyssen et al. (2017) may not be appropriate for specifically silencing the expression of the target actin gene. In plants, VIGS can reduce the expression of endogenous genes that are homologous to the inserted fragment in the VIGS vector *via* RNA-mediated defense (RMD) mechanisms (Baulcombe, 1999). RMD recognizes the complementary RNA sequence by base pairing, thus unintended off-target genes may also be silenced if they share high sequence similarity with the inserted fragment, and the interpretation of the observed phenotypic changes may be consequently obscured (Senthilkumar and Mysore, 2011). In fact, this phenomenon has long been attracted the attention of researchers (Burch-Smith et al., 2004; Xu et al., 2006; Fantini et al., 2013; Kumar, 2014). To specifically known down the expression of an actin gene, *GhACT1*, in cotton, researchers have used its gene-specific 3'-UTR fragment for RNAi vector construction (Li et al., 2005). However, a conserved fragment could simultaneously knockdown the expression of other members of a gene family or other genes that share high sequence similarity with the trigger sequence (Ramachandran et al., 2000; Burch-Smith et al., 2004; Kandoth et al., 2007). Our present analysis of the actin family genes in *G. hirsutum* showed that the CDS of *GhACTs* share more than 80% sequence similarity with each other (**Supplementary Figure S5**). This is high enough for efficient gene silencing (Holzberg et al., 2002; Zhai et al., 2016). Secondly, the use of receptor plants in the VIGS experiment by Thyssen et al. (2017) is not suitable. Genetic study has proved that the Li₁ mutant was caused by a semi-dominant gene, thus

the "gain-of-function" gene *Li₁* is required for the formation of the mutant phenotype in Li₁. To verify the function of *Li₁*, phenotypic changes in Li₁ plants after silencing of the dominant gene *Li₁* should be examined, since phenotypic changes in the WT plants after the reduced expression of the recessive gene cannot represent the function of *Li₁*. This principle is supported by many previous RNAi and VIGS studies, such as those in rice (Huang et al., 2009; Jiao et al., 2010; Tang et al., 2011; Li et al., 2015) and cotton (Chang et al., 2016; Si et al., 2018).

To investigate whether the mutated actin gene *Gh_D04G0865* is the gene underlying the *Li₁* locus, we firstly attempted to develop transgenic lines that overexpress the mutated *Gh_D04G0865* driven by the 35S promoter in WT cotton line W0 (Wu et al., 2008). However, we failed to generate positive plant with the expressed target gene, probably due to the detrimental effects on cell elongation of the mutated *Gh_D04G0865*. To investigate whether the mutated *Gh_D04G0865* is responsible for the Li₁ mutant, and at the same time to verify our different opinions with Thyssen et al. (2017), we performed two groups of VIGS experiments. One fragment corresponding to 730–1121-bp CDS (shares higher than 81.22% sequence similarity with other *GhACTs*) and another corresponding to 1–297-bp 3'UTR of *Gh_D04G0865* were separately cloned into pTRV2 vector, generating pTRV2::CDS (TRV : CDS) and pTRV2::UTR (TRV : UTR) constructs. Li₁ and WT seedlings were used as receptors to observe their phenotypic changes after VIGS treatment. Fifteen days after inoculation, the newly grown leaves were used for phenotypic observation since the morphology of older leaves had already formed before VIGS treatment. Leaves from all TRV : UTR treated WT plants had little change in comparison to that from untreated and TRV:00 (empty vector for control) treated WT plants (**Figure 3E**), probably due to the functional redundancy of actin genes as reported in Arabidopsis (for example: *act2*, *act4*, and *act7* T-DNA mutants showed little phenotype changes; Gilliland et al., 1998). Compared with untreated and TRV:00 treated Li₁ plants, more flatten leaves were observed in 55 out of 60 TRV : UTR treated plants (**Figure 3E**). In contrast, very seriously deformed leaves were produced from 55 out of 60 TRV : CDS treated Li₁, and 57 out of 60 TRV : CDS treated WT plants in TRV : CDS treated Li₁ and WT plants, and this phenotype was radically different with untreated Li₁ leaves (**Figure 3E**). Moreover, viability of these plants became too weak to produce the third true leaf. qRT-PCR was used to determine the expression level of nine-leaf-expression *GhACTs* as indicated by the transcriptomic data (**Supplementary Figures S6** and **S8**). As we expected, only *Gh_D04G0865* was significantly silenced
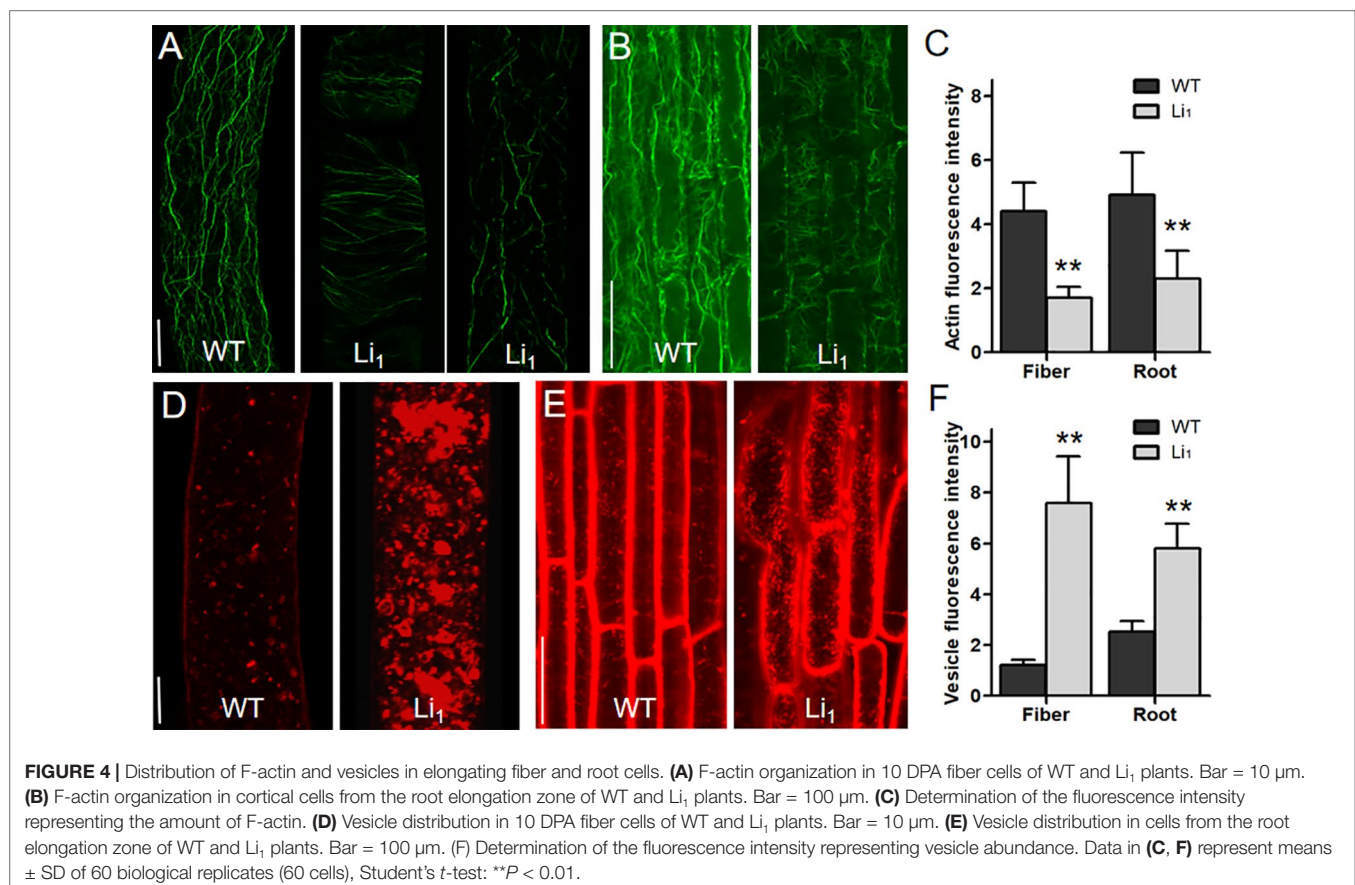
in TRV : UTR treated Li_1 and WT plants. In contrast, TRV : CDS significantly reduced the expression level of all of the tested *GhACTs* in Li_1 and WT plants. These results demonstrated that this VIGS phenotype could not be used to explain the function of the targeted gene. Phenotypic changes in the VIGS experiment were more obvious at 90 days after treatment: TRV : UTR treated WT plants had little difference with untreated and TRV:00 treated plants; TRV : UTR treated Li_1 plants exhibited relieved mutant phenotype characterized by taller plants (**Figure 3F**), more flatten leaves and straighter stems than that from two groups of control plants (**Figure 3G**). Expression level of *Gh_D04G0865* in the leaves and stems from TRV : UTR treated plants were significantly decreased (**Figure 3H**). These results suggested that the mutated *Gh_D04G0865* expression was tightly linked to the degree performance of Li_1 plants and confirmed that the mutated *Gh_D04G0865* was responsible for the Li_1 mutant. Given the dominant inherited feature of the Li_1 mutants, *Gh_D04G0865* was named *Ghli_1* and *GhLi_1* for the wild and mutant types, respectively.

Changes in Actin Cytoskeleton and Vesicle Distribution in Elongating Cells

Although it is clear that *GhLi_1* encodes a mutated actin, the mechanisms by which the G65V substituted actin affects the organization of the actin cytoskeleton in elongating cells remains

to be explored. In 10 DPA fibers, which undergo fast elongation, many fine F-actin cables were formed, and further arranged longitudinally to the axis of the fiber cell in the WT (**Figure 4A**). However, the F-actin cables in 10 DPA Li_1 fibers were arranged horizontally or obliquely, and their distribution was obviously sparser than that of the WT. In some cases, F-actin cables in the Li_1 fiber cells were fragmented (**Figure 4A**). The same differences in the organization of the F-actin cytoskeleton between the Li_1 mutants and the WT were observed in cortical cells from the root elongation zone (**Figure 4B**). A quantitative measurement of the fluorescence intensity of the confocal images showed that the amount of F-actin in the Li_1 elongating root and fiber cells was significantly lower than that in the WT (**Figure 4C**).

The actin cytoskeleton has been found to serve as tracks for intracellular transportation (Gutierrez et al., 2009). To investigate whether the intracellular transportation in the Li_1 cells is affected, the distribution of vesicles in elongating fiber and root cells was observed. FM4-64 staining showed that vesicles were distributed evenly in the WT fiber cells; however, massive vesicles aggregated into patches were observed in the Li_1 fiber cells (**Figure 4D**). Similarly, more labeled vesicles were present in the Li_1 cells from root elongation zone than that in the WT (**Figure 4E**). Measurement of the fluorescence intensity showed significantly more vesicles in the Li_1 elongating root and fiber cells than in the WT (**Figure 4F**). These observations suggest that intracellular transportation was disturbed in the Li_1 elongating cells.

FIGURE 4 | Distribution of F-actin and vesicles in elongating fiber and root cells. **(A)** F-actin organization in 10 DPA fiber cells of WT and Li_1 plants. Bar = 10 μm. **(B)** F-actin organization in cortical cells from the root elongation zone of WT and Li_1 plants. Bar = 100 μm. **(C)** Determination of the fluorescence intensity representing the amount of F-actin. **(D)** Vesicle distribution in 10 DPA fiber cells of WT and Li_1 plants. Bar = 10 μm. **(E)** Vesicle distribution in cells from the root elongation zone of WT and Li_1 plants. Bar = 100 μm. (F) Determination of the fluorescence intensity representing vesicle abundance. Data in **(C)**, **F)** represent means ± SD of 60 biological replicates (60 cells), Student's *t*-test: **$P < 0.01$.

Changes in the Distribution of the Actin Cytoskeleton, Vesicles, and CSC in Fiber Cells During SCW Biosynthesis

The more thickened SCW and higher cellulose content of Li_1 fibers compared to WT fibers (**Figures 2G–J**) offers an ideal model for investigating the role of the actin cytoskeleton in SCW biosynthesis. We therefore examined whether the distribution of the actin cytoskeleton, vesicles, and CSC were affected in Li_1 fiber cells at 20 DPA, when they undergo active SCW biosynthesis. As shown in **Supplementary Figure S9A**, the F-actin cables in the WT fiber cells became thick and straight; while fewer thick F-actin cables were formed, and those that did were fragmented and randomly arranged in the Li_1 fiber cells. As in elongating fibers, vesicles in the Li_1 fiber cells were aggregated into patches during SCW biosynthesis, a distribution dramatically different to that in corresponding WT fiber cells (**Supplementary Figure S9B**). To determine the CSC distribution in the Li_1 and WT fibers, the commercial antibody anti-CesA4 was used for immunostaining experiments (Gardiner et al., 2003). As shown in **Supplementary Figure S9C**, the distribution of CSC was obviously increased in the Li_1 fibers in comparison to the WT. Quantitative analysis showed the amount of F-actin was significantly reduced, while the number of vesicles and CSC were significantly increased in the Li_1 fiber cells (**Supplementary Figure S9D–F**). Based on these results, we propose that the disturbed intracellular transportation and excessive distribution of CSC at the PM is the major reasons for the increased content of cellulose and thickened SCW of Li_1 fiber cells.

Effects of G65V Substitution on Actin Polymerization

Amino acid substitution in a protein as conserved as actin may dramatically affect its function, thus we investigated the influence of the G65V substitution in $GhLi_1$. An extensive protein sequence alignment showed that the 65G was highly conserved in actin (**Supplementary Figure S10** and **Supplementary Table S5**), indicating that it may be necessary for actin's basic function. The 65G is located on the surface-exposed region of subdomain 2, also known as a junction among G-actins in an F-actin (**Figures 5A–C**; Holmes et al., 1990). Simulation of G65V substitution in the F-actin molecule gave rise to a steric hindrance and a hydrogen bond between the 65V in molecule A and the 175H and 288D in molecule C, respectively (**Figures 5D, E**). Holmes et al. (1990) reported the atomic structure of F-actin and proposed that the hydrophobic "plug-pocket" interaction is essential for F-actin stabilization. According to the structural correspondence between the protein sequences of $GhLi_1$ and the rabbit skeletal muscle actin used in the "Holmes model", the occurrence of "plug-pocket" interactions in cotton actin can be depicted as shown in **Figure 5C**. In a normal F-actin, eight residues (positions 42–47, 65, and 66) of molecule A and six residues (positions 168, 171, 173, 175, 287, and 291) of molecule C form a hydrophobic pocket. At the same time, a hydrophobic loop (residues 266–275) of molecule B in the opposing strand generates a hydrophobic plug, which inserts into the hydrophobic pocket to bring about a strong three-bodied G-actin interaction. Moreover, some salt
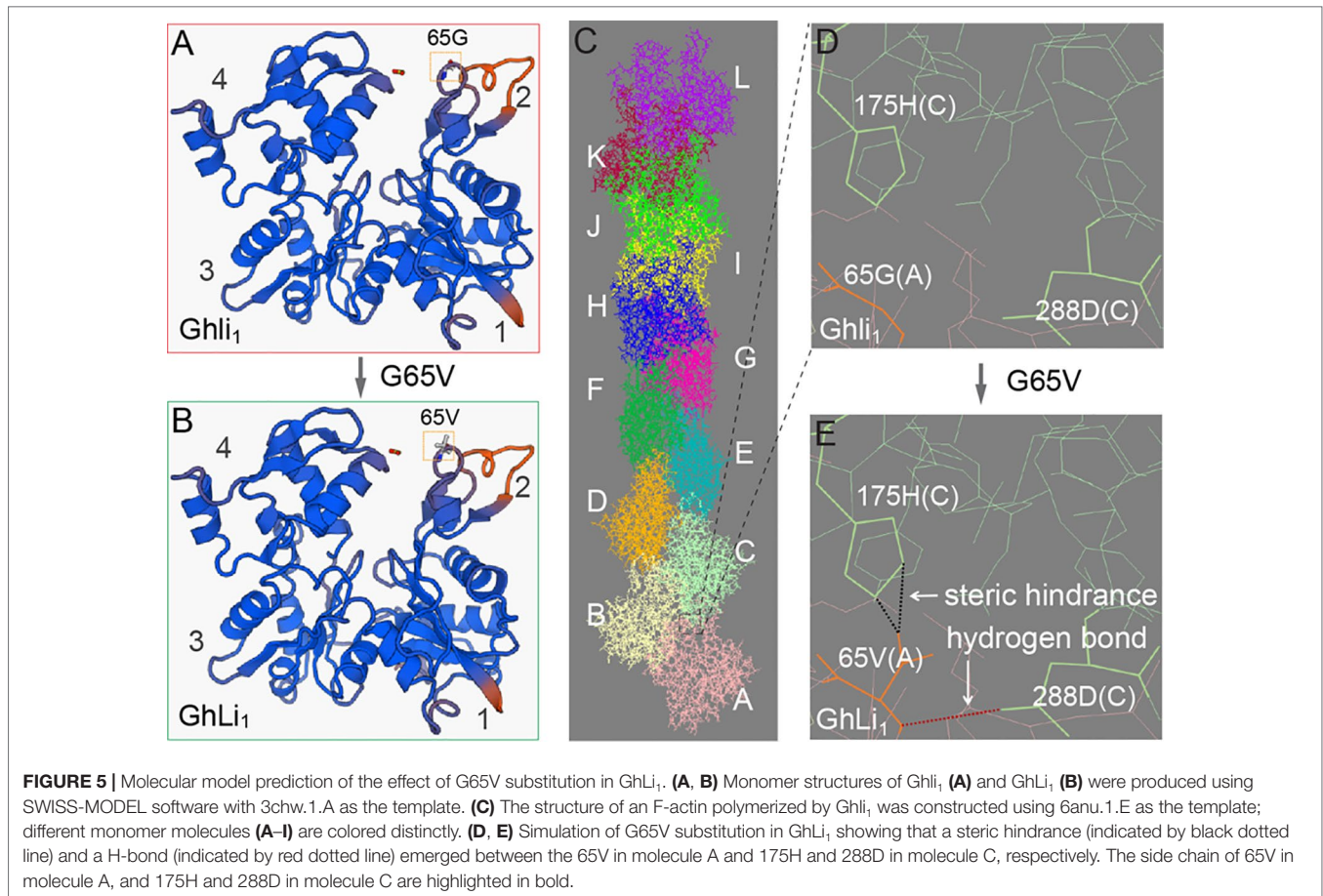
bridges are formed near this interaction zone to stabilize the F-actin structure, including one between the 41R of molecule A and the 288D of molecule C. According to our model, the steric hindrance and hydrogen bond caused by G65V substitution may affect the three-bodied G-actin interaction by changing the structure of the hydrophobic pocket and influencing the formation of the salt bridge, leading to instability of the F-actin.

We next produced 6×His-tag fused $GhLi_1$ and $Ghli_1$ proteins to investigate their functional differences through *in vitro* biochemical assays (**Figure 6A**). To generate a new F-actin, three G-actin molecules must interact to create a seed, which is the rate-limiting step during spontaneous F-actin assembly (Pollard and Cooper, 1986). We performed *in vitro* analysis using the recombinant $GhLi_1$ and $Ghli_1$ proteins to test their nucleation ability. Actin monomers (10% pyrene labeled) from rabbit skeletal muscle were incubated with different concentrations of $GhLi_1$ and $Ghli_1$, and the actin assembly status was monitored by pyrene fluorescence measurement. As shown in **Figure 6B** and **Supplementary Table S6**, $Ghli_1$ decreased the initial lag of the actin polymerization curve in a dose-dependent manner, which is indicative of their active roles in actin nucleation (Michelot et al., 2005). In contrast, the initial lag of the actin polymerization curve was increased as the increase of $GhLi_1$ concentration, indicating that $GhLi_1$ disturbs actin nucleation. The final amplitude of pyrene fluorescence, which is directly proportional to the actin filament concentration, was dramatically decreased with the addition of $GhLi_1$, suggesting that actin polymerization was disturbed by this mutated actin.

To further investigate the polymerization capability of the recombinant $GhLi_1$ and $Ghli_1$ proteins, we observed actin filaments under fluorescence microscope. After 5-min polymerization, $Ghli_1$ produced a large number of short actin filaments, whereas there were significantly fewer actin filaments produced from the mixture of $Ghli_1$ and $GhLi_1$, and $GhLi_1$ alone did not produce any actin filaments under the same conditions (**Figures 6C, D**). After 20-min polymerization, $Ghli_1$ produced long actin filaments, whereas actin filaments from the mixture of $Ghli_1$ and $GhLi_1$ were significantly shorter, and no actin filaments were produced by $GhLi_1$ (**Figures 6E, F**). These results further confirm that $GhLi_1$ disturbs nucleation and elongation of F-actin. Thus, it is fully reasonable to infer that the polymerization status in tissues with $GhLi_1$ expression in the Li_1 differs to that in the WT. We propose that, in the Li_1 cells, $GhLi_1$ could partake in, but disturbed, actin's physical interactions (**Figure 6G**). When $GhLi_1$ was involved in nucleation, normal seeds could not be formed. When $GhLi_1$ was added onto the elongating end of an F-actin molecule by chance, it inhibited further polymerization by creating a "dead end".

DISCUSSION

The actin cytoskeleton plays important roles in almost all cellular processes (Staiger et al., 2000; Blanchoin et al., 2010). Mutations in actin cause a range of malformed morphologies due to specific molecular changes that often disturb cytoskeleton functions (Feng and Marston, 2009; Kato et al., 2010). In this study, we report the
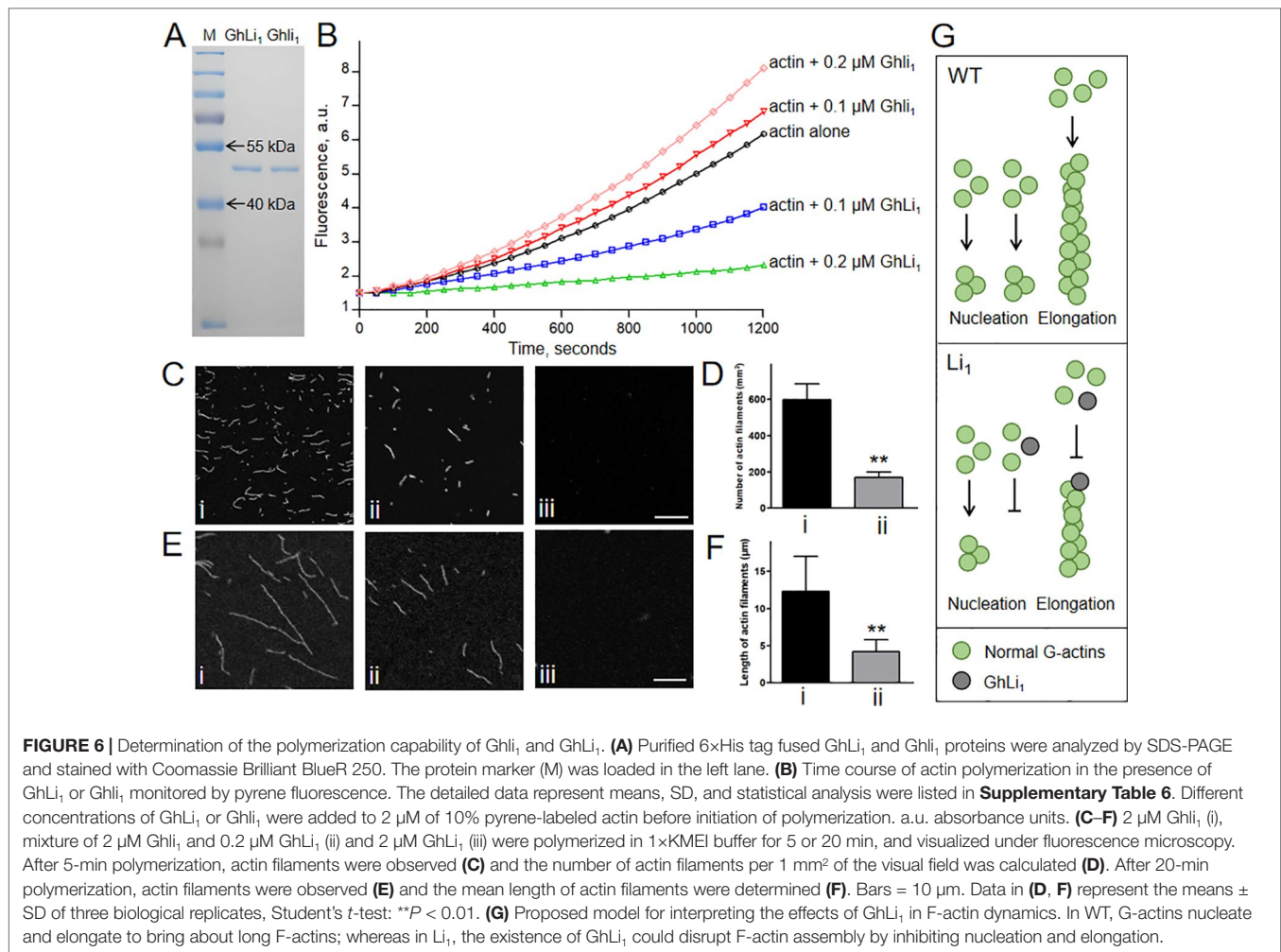
FIGURE 5 | Molecular model prediction of the effect of G65V substitution in GhLi$_1$. **(A, B)** Monomer structures of Ghli$_1$ **(A)** and GhLi$_1$ **(B)** were produced using SWISS-MODEL software with 3chw.1.A as the template. **(C)** The structure of an F-actin polymerized by Ghli$_1$ was constructed using 6anu.1.E as the template; different monomer molecules **(A–I)** are colored distinctly. **(D, E)** Simulation of G65V substitution in GhLi$_1$ showing that a steric hindrance (indicated by black dotted line) and a H-bond (indicated by red dotted line) emerged between the 65V in molecule A and 175H and 288D in molecule C, respectively. The side chain of 65V in molecule A, and 175H and 288D in molecule C are highlighted in bold.

isolation and characterization of *GhLi$_1$*, which encodes a mutated actin with a G65V substitution in its gene product, from the Li$_1$ mutants. Our results demonstrate that GhLi$_1$ disorders actin cytoskeleton organization and intracellular transportation, and consequently alters the morphogenesis of cotton plants and cells.

The Actin Cytoskeleton Plays Crucial Roles in Cell Elongation and the SCW Biosynthesis in Cotton

Actin cytoskeleton has been reported to essential for plant morphology. Previous studies had showed that disorganized actin cytoskeleton caused by pharmacological perturbation, mutation, or misexpression of actin and actin cytoskeleton-associated genes inhibited cell growth and altered the plant architecture (Kato et al., 2010; Wu et al., 2015). Cotton is a mainstay of the global economy and is prized for its excellent natural fiber properties. In this study, we showed that the dominant mutated actin gene *GhLi$_1$* disorganized actin cytoskeleton, disrupts proper cell elongation, and resulted in various twisted organs. Thus, this report establishes that the mutation of a single actin can cause dramatic morphogenetic defects in cotton. Many studies have found that the actin cytoskeleton regulates cotton fiber development. Reduction in F-actin abundance inhibits fiber elongation (Seagull, 1990;

Li et al., 2005), while thicker and more abundant F-actin cables promote fiber length and strength (Wang et al., 2009; Wang et al., 2010; Zhang et al., 2017). In this study, we found that the F-actin cables in Li$_1$ were disorganized and fragmented (**Figure 4** and **Supplementary Figure S9**), which resulted in shortened and thickened fiber cells (**Figure 2**). Our findings provide solid genetic evidence of the pivotal roles of the actin cytoskeleton in regulating cotton fiber development.

During cell growth, vesicles containing cell wall matrix materials are delivered to expansion sites and fuse with the PM to deposit their contents to the cell wall (Ketelaar et al., 2003). Previous studies proposed that longitudinally oriented actin cables were the primary tracks for organelle movement (Gutierrez et al., 2009; Kato et al., 2010; Akkerman et al., 2012). During the fast elongation stage, cotton fibers undergo enormous polar growth, while massive cellulose molecules are synthesized during SCW deposition stage (Haigler et al., 2012). Thus, active cellular transport must take place in fiber cells during these development stages. It is conceivable that the reduction in longitudinal actin cables in the Li$_1$ cells leads to abnormal vesicle transportation. Indeed, our cytological observations showed that vesicles were aggregated into patches, and more CSCs were inserted into the PM of Li$_1$ cells than that of WT, which inhibited cell elongation and caused excessive cellulose deposition (**Figure 4** and **Supplementary Figure S9**). Based on these results, we

FIGURE 6 | Determination of the polymerization capability of Ghli₁ and GhLi₁. **(A)** Purified 6×His tag fused GhLi₁ and Ghli₁ proteins were analyzed by SDS-PAGE and stained with Coomassie Brilliant BlueR 250. The protein marker (M) was loaded in the left lane. **(B)** Time course of actin polymerization in the presence of GhLi₁ or Ghli₁ monitored by pyrene fluorescence. The detailed data represent means, SD, and statistical analysis were listed in **Supplementary Table 6**. Different concentrations of GhLi₁ or Ghli₁ were added to 2 μM of 10% pyrene-labeled actin before initiation of polymerization. a.u. absorbance units. **(C–F)** 2 μM Ghli₁ (i), mixture of 2 μM Ghli₁ and 0.2 μM GhLi₁ (ii) and 2 μM GhLi₁ (iii) were polymerized in 1×KMEI buffer for 5 or 20 min, and visualized under fluorescence microscopy. After 5-min polymerization, actin filaments were observed **(C)** and the number of actin filaments per 1 mm² of the visual field was calculated **(D)**. After 20-min polymerization, actin filaments were observed **(E)** and the mean length of actin filaments were determined **(F)**. Bars = 10 μm. Data in **(D, F)** represent the means ± SD of three biological replicates, Student's t-test: **P < 0.01. **(G)** Proposed model for interpreting the effects of GhLi₁ in F-actin dynamics. In WT, G-actins nucleate and elongate to bring about long F-actins; whereas in Li₁, the existence of GhLi₁ could disrupt F-actin assembly by inhibiting nucleation and elongation.

hypotheses that F-actin may acts as a track for vesicle movement thus regulating elongation and SCW deposition in fiber cells.

G65V Substitution in Actin Disturbs F-Actin Assembly

Actin is one of the most ancient proteins that is essential for the survival of eukaryotes. In accordance with actin's high evolutionary conservation, most amino acid residues are critical for actin's function. Over the past few decades, hundreds of actin mutants, responsible for various morphological changes, have been identified in both uni- and multi-cellular organisms (Ishiguro and Kobayashi, 1996; Feng and Marston, 2009; Kato et al., 2010). Actin mutants in human are the most thoroughly studied because they are causal for genetic diseases (Pierick et al., 2014; Marston, 2018). At the molecular level, these mutated actins were unable to fold properly to form functional actin, were incapable of polymerization, or had changes in their ability to interact with ABPs (Costa et al., 2004; Feng and Marston, 2009). With the availability of abundant information for actin mutants, a framework for genotype-phenotype correlation could be built and used for molecular diagnosis of human diseases (Marston, 2018),

and also probably for the characterization of abnormal developments of animals and plants in view of the functional conservation of actin cytoskeleton. Prediction on the possible effects of each mutation based on its structural location and our knowledge of actin structure-function relationships is an efficient approach in understanding of their molecular mechanisms.

According to the Holmes model, the hydrophobic "plug-pocket" structure constitutes a three-bodied interaction that is essential for F-actin stability (Holmes et al., 1990). Many amino acid substitutions in, or near, this region exhibit different effects, for example I64N, T66I, G268C, D286G, and D291V in human skeletal actin ACTA1 exhibited reduced or completely lost polymerization capability, and resulted in various congenital myopathies (Feng and Marston, 2009). G273D in yeast actin ACT1 give rise to abnormal cell growth, probably because the amino acid substitution affects the hydrophobic "plug-pocket" interaction (Ishiguro and Kobayashi, 1996), and similar structural changes were proposed in E272K in Arabidopsis ACT8 (Kato et al., 2010). Position 65 in GhLi₁, which is structurally identical to position 63 in the rabbit actin used by Holmes et al. (1990), participates in the hydrophobic "pocket" formation. Mutation in this

position is novel and different from previously reported actin mutants. According to our model, the steric hindrance and hydrogen bond caused by G65V substitution may affect the three-bodied interaction by changing the hydrophobic pocket structure and influencing the formation of the salt bridge, which could be unfavorable for F-actin assembly (**Figure 5**; Holmes et al., 1990). Our biochemical assays demonstrated that GhLi$_1$ was completely lost polymerization capability. In addition, it also inhibited nucleation and elongation activities normally occurred in F-actin assembly process (**Figure 6**). Thus, G65V substitution may converts GhLi$_1$ from a normal linker to a "disturbing or capping protein". Our results are in agreement with previous studies on actin mutants, and provide a new genotype-phenotype example of deciphering the process of abnormal development in plants. This model may also be useful for other eukaryotes.

DATA AVAILABILITY STATEMENT

The datasets generated for this study are available on request to the corresponding author.

REFERENCES

Akkerman, M., Overdijk, E. J., Schel, J. H., Emons, A. M., and Ketelaar, T. (2012). Golgi body motility in the plant cell cortex correlates with actin cytoskeleton organization. *Plant Cell Physiol.* 52, 1844–1855. doi: 10.1093/pcp/pcr122

Bao, Y., Hu, G. J., Flagel, L. E., Salmon, A., Bezanilla, M., Paterson, A. H., et al. (2011). Parallel up-regulation of the profilin gene family following independent domestication of diploid and allopolyploid cotton (*Gossypium*). *Proc. Natl. Acad. Sci. U. S. A.* 108, 21152–21157. doi: 10.1073/pnas.1115926109

Baulcombe, D. C. (1999). Fast forward genetics based on virus induced gene silencing. *Curr. Opin. Cell Biol.* 2, 109–113. doi: 10.1016/S1369-5266(99)80022-3

Blanchoin, L., Boujemaa-Paterski, R., Henty, J. L., Khurana, P., and Staiger, C. (2010). Actin dynamics in plant cells: a team effort from multiple proteins orchestrates this very fast-paced game. *Curr. Opin. Cell Biol.* 13, 714–723. doi: 10.1016/j.pbi.2010.09.013

Bryan, K. E., Wen, K. K., Zhu, M., Rendtorff, N. D., Feldkamp, M., Tranebjaerg, L., et al. (2006). Effects of human deafness gamma-actin mutations (*DFNA20/26*) on actin function. *J. Biol. Chem.* 281, 20129–20139. doi: 10.1074/jbc.M601514200

Burch-Smith, T. M., Anderson, J. C., Martin, G. B., and Dinesh-Kumar, S. P. (2004). Applications and advantages of virus-induced gene silencing for gene function studies in plants. *Plant J.* 39, 734–746. doi: 10.1111/j.1365-313x.2004.02158.x

Chang, L., Fang, L., Zhu, Y. J., Wu, H. T., Zhang, Z. Y., Liu, C. X., et al. (2016). Insights into interspecific hybridization events in allotetraploid cotton formation from characterization of a gene regulating leaf shape. *Genetics* 204, 799–806. doi: 10.1534/genetics.116.193086

Chen, C. Y., Wong, E. I., Vidali, L., Estavillo, A., Helper, P. K., Wu, H. M., et al. (2002). The regulation of actin organization by actin-depolymerizing factor in elongating pollen tubes. *Plant Cell* 14, 2175–2190. doi: 10.1105/tpc.003038

Chen, N. Z., Qu, X. L., Wu, Y. J., and Huang, S. J. (2009). Regulation of actin dynamics in pollen tubes: control of actin polymer level. *J. Integer. Plant Biol.* 51, 740–750. doi: 10.1111/j.1744-7909.2009.00850.x

Costa, C. F., Rommelaere, H., Waterschoot, D., Sethi, K. K., Nowak, K. J., Laing, N. G., et al. (2004). Myopathy mutations in alpha-skeletal-muscle actin cause a range of molecular defects. *J. Cell Sci.* 117, 3367–3377. doi: 10.1242/jcs.01172

Deng, W. K., Wang, Y. B., Liu, Z. X., Cheng, H., and Xue, Y. (2014). HemI: a toolkit for illustrating heatmaps. *PloS One* 9, e111988–111993. doi: 10.1371/journal.pone.0111988

AUTHOR CONTRIBUTIONS

TZ conceptualized the research program. TZ and YH designed the experiments and coordinated the project. YS, WL, WS, HF, and ZS conducted map-based cloning and functional analysis of the *Li$_1$* gene. YS and JC developed the molecular markers. YS, YH, and TZ analyzed all of the data and wrote the paper.

FUNDING

SUPPLEMENTARY MATERIAL

The Supplementary Material for this article can be found online at: https://www.frontiersin.org/articles/10.3389/fpls.2019.01486/full#supplementary-material

Emons, A. M. C., and Ketelaar, T. (2009). Intracellular organization: a prerequisite for root hair elongation and cell wall deposition. Root Hairs, (Berlin, Heidelberg, New York: Springer), 12, 69–86. doi: 10.1007/7089_2008_4

Fantini, E., Falcone, G., Frusciante, S., Giliberto, L., and Giuliano, G. (2013). Dissection of tomato lycopene biosynthesis through virus-induced gene silencing. *Plant Physiol.* 163, 986–998. doi: 10.1104/pp.113.224733

Feng, J. J., and Marston, S. (2009). Genotype-phenotype correlations in ACTA1 mutations that cause congenital myopathies. *Neuromuscul. Disord.* 19, 6–16. doi: 10.1016/j.nmd.2008.09.005

Gao, X. Q., Wheeler, T., Li, Z. H., Kenerley, C. M., He, P., and Shan, L. B. (2011). Silencing *GhNDR1* and *GhMKK2* compromises cotton resistance to *Verticillium wilt*. *Plant J.* 66, 293–305. doi: 10.1111/j.1365-313X.2011.04491.x

Gardiner, J. C., Taylor, N. G., and Turner, S. R. (2003). Control of cellulose synthase complex localization in developing xylem. *Plant Cell* 15, 1740–1748. doi: 10.1105/tpc.012815

Gilbert, M. K., Turley, R. B., Kim, H. J., Li, P., Thyssen, G., Tang, Y. H., et al. (2013). Transcript profiling by microarray and marker analysis of the short cotton (*Gossypium hirsutum* L.) fiber mutant Ligon lintless-1 (Li$_1$). *BMC Genomics* 14, 403–403. doi: 10.1186/1471-2164-14-403

Gilliland, L. U., Mckinney, E. C., Asmussen, M. A., and Meagher, R. B. (1998). Detection of deleterious genotypes in multigenerational studies. I. Disruptions in individual Arabidopsis actin genes. *Genetics* 149, 717–725. doi: 10.1017/S0016672398003267

Griffee, F., and Ligon, L. L. (1929). Occurrence of lintless cotton plants and the inheritance of the character lintless. *J. Am. Soc Agron.* 21, 711–717. doi: 10.2134/agronj1929.00021962002100070001x

Guex, N., Peitsch, M. C., and Schwede, T. (2009). Automated comparative protein structure modeling with SWISS-MODEL and Swiss-PdbViewer: a historical perspective. *Electrophoresis* 30, 162–173. doi: 10.1002/elps.200900140

Gutierrez, R., Lindeboom, J. J., Paredez, A. R., Emons, A. M., and Ehrhardt, D. W. (2009). Arabidopsis cortical microtubules position cellulose synthase delivery to the plasma membrane and interact with cellulose synthase trafficking compartments. *Nat. Cell Biol.* 11, 797–806. doi: 10.1038/ncb1886

Haigler, C. H., Lissete, B., Stiff, M. R., and Tuttle, J. R. (2012). Cotton fiber: a powerful single-cell model for cell wall and cellulose research. *Front. Plant Sci.* 3, 104–110. doi: 10.3389/fpls.2012.00104

Han, L. B., Li, Y. B., Wang, H. Y., Wu, X. M., Li, C. L., Luo, M., et al. (2013). The dual functions of WLIM1a in cell elongation and secondary wall formation in developing cotton fibers. *Plant Cell* 25, 4421–4438. doi: 10.1105/tpc.113.116970

Holmes, K. C., Popp, D., Gebhard, W., and Kabsch, W. (1990). Atomic model of the actin filament. *Nature* 347, 44–49. doi: 10.1038/347044a0

Holzberg, S., Brosio, P., Gross, C., and Pogue, G. P. (2002). *Barley stripe mosaic virus*-induced gene silencing in a monocot plant. *Plant J.* 30, 315–327. doi: 10.1046/j.1365-313X.2002.01291.x

Huang, X. Z., Qian, Q., Liu, Z. B., Sun, H. Y., He, S. Y., Luo, D., et al. (2009). Natural variation at the *DEP1* locus enhances grain yield in rice. *Nat. Genet.* 41, 494–497. doi: 10.1038/ng.352

Hussey, P. J., Ketelaar, T., and Deeks, M. J. (2006). Control of the actin cytoskeleton in plant cell growth. *Annu. Rev. Plant Biol.* 57, 109–125. doi: 10.1146/annurev.arplant.57.032905.105206

Ishiguro, J., and Kobayashi, W. (1996). An actin point-mutation neighboring the 'hydrophobic plug' causes defects in the maintenance of cell polarity and septum organization in the fission yeast *Schizosaccharomyces pombe*. *FEBS Lett.* 392, 237–241. doi: 10.1016/0014-5793(96)00819-8

Jiang, Y. R., Ding, M. Q., Cao, Y. F., Yang, F., Zhang, H., He, S. E., et al. (2015). Genetic fine mapping and candidate gene analysis of the *Gossypium hirsutum* Ligon lintless-1 (*Li₁*) mutant on chromosome 22(D). *Mol. Genet. Genomics* 290, 2199–2211. doi: 10.1007/s00438-015-1070-2

Jiao, Y. Q., Wang, Y. H., Xue, D. W., Wang, J., Yan, M. X., Liu, G. F., et al.(2010). Regulation of *OsSPL14* by OsmiR156 defines ideal plant architecture in rice. *Nat. Genet.* 42, 541–544. doi: 10.1038/ng.591

Kandoth, P. K., Ranf, S., Pancholi, S. S., Jayanty, S., Walla, M. D., Miller, W., et al. (2007). Tomato MAPKs LeMPK1, LeMPK2, and LeMPK3 function in the systemin-mediated defense response against herbivorous insects. *Proc. Natl. Acad. Sci. U. S. A.* 104, 12205–12210. doi: 10.1073/pnas.0700344104

Karaca, M., Saha, S., Jenkins, J. N., Zipf, A., Kohel, R., and Stelly, D. M. (2002). Simple sequence repeat (SSR) markers linked to the Ligon lintless (Li₁) mutant in cotton. *J. Hered.* 93, 221–224. doi: 10.1093/jhered/93.3.221

Kato, T., Morita, M. T., and Tasaka, M. (2010). Defects in dynamics and functions of actin filament in Arabidopsis caused by the dominant-negative actin *fiz1*-induced fragmentation of actin filament. *Plant Cell Physiol.* 51, 333–338. doi: 10.1093/pcp/pcp189

Ketelaar, T., Ruijter, N. C., and Emons, A. M. (2003). Unstable F-Actin specifies the area and microtubule direction of cell expansion in Arabidopsis root hairs. *Plant Cell* 15, 285–292. doi: 10.1105/tpc.007039

Kohel, R. J. (1972). Linkage tests in upland cotton, *Gossypium hirsutum* L. II. *Crop Sci.* 5, 66–69. doi: 10.2135/cropsci1965.0011183X000500060029x

Kumar, S. (2014). RNAi (RNA Interference) vectors for functional genomics study in plants. *Natl. Acad. Sci. Lett.* 37, 289–294. doi: 10.1007/s40009-014-0234-7

Larkin, M. A., Blackshields, G., Brown, N. P., Chenna, R., McGettigan, P. A., McWilliam, H., et al. (2007). Clustal W and Clustal X version 2.0. *Bioinformatics* 23, 2947–2948. doi: 10.1093/bioinformatics/btm404

Li, X. B., Fan, X. P., Wang, X. L., Cai, L., and Yang, W. C. (2005). The cotton *ACTIN1* gene is functionally expressed in fibers and participates in fiber elongation. *Plant Cell* 17, 859–875. doi: 10.1105/tpc.104.029629

Li, Y., Jiang, J., Li, L., Wang, X. L., Wang, N. N., Li, D. D., et al. (2013). A cotton LIM domain-containing protein (GhWLIM5) is involved in bundling actin filaments. *Plant Physiol. Biochem.* 66, 34–40. doi: 10.1016/j.plaphy.2013.01.018

Li, G., Liang, W. Q., Zhang, X. Q., Ren, H. Y., Hu, J. P., Bennett, M. J., et al. (2014). Rice actin-binding protein RMD is a key link in the auxin-actin regulatory loop that controls cell growth. *Proc. Natl. Acad. Sci. U. S. A.* 111, 10377–10382. doi: 10.1073/pnas.1401680111

Li, X. M., Chao, D. Y., Wu, Y., Huang, X. H., Chen, K., Cui, L. G., et al. (2015). Natural alleles of a proteasome α2 subunit gene contribute to thermotolerance and adaptation of African rice. *Nat. Genet.* 47, 827–833. doi: 10.1038/ng.3305

Li, Y., Wang, N. N., Wang, Y., Liu, D., Gao, Y., Li, L., et al. (2018). The cotton XLIM protein (GhXLIM6) is required for fiber development *via* maintaining dynamic F-actin cytoskeleton and modulating cellulose biosynthesis. *Plant J.* 96, 1269–1282. doi: 10.1111/tpj.14108

Liang, W., Fang, L., Xiang, D., Hu, Y., Feng, H., Chang, L. J., et al. (2015). Transcriptome analysis of short fiber mutant Ligon lintless-1 (Li₁) reveals critical genes and key pathways in cotton fiber elongation and leaf development. *PloS One* 10, e0143503–0143521. doi: 10.1371/journal.pone.0143503

Liang, W.(2015). Fine-mapping of short fiber mutant gene *Li₁* and transcriptome analysis of Ligon lintless-1 (Li₁) mutant in Upland cotton. Nanjing: Doctoral dissertation of Nanjing Agriculture University (in Chinese with English abstract).

Liu, F. J., Liang, W. H., and Zhang, T. Z. (2010). Genetic analysis of homozygous-dominant-surviving Ligon lintless recombinants in cotton (*Gossypium hirsutum* L.). *Acta Agron. Sin.* 36, 2020–2027. doi: 10.1016/s1875-2780(09)60086-9

Liu, X., Zhao, B., Zheng, H. J., Hu, Y., Lu, G., Yang, C. Q., et al. (2015). Gossypium barbadense genome sequence provides insight into the evolution of extra-long staple fiber and specialized metabolites. *Sci. Rep.* 5 (1), 14139–14152. doi: 10.1038/srep14139

Marston, S. (2018). The molecular mechanisms of mutations in actin and myosin that cause inherited myopathy. *Int. J. Mol. Sci.* 19, 2020–2037. doi: 10.3390/ijms19072020

Mathur, J., and Martin, H. (2002). Microtubules and microfilaments in cell morphogenesis in higher plants. *Curr. Biol.* 12, 669–676. doi: 10.1016/s0960-9822(02)01164-8

McDowell, J. M., Huang, S. R., Mckinney, E. C., An, Y. Q., and Meagher, R. B. (1996). Structure and evolution of the actin gene family in *Arabidopsis thaliana*. *Genetics* 142, 587–602. doi: 10.1073/pnas.79.2.495

Meagher, R. B., Mckinney, E. C., and Kandasamy, M. K. (1999). Isovariant dynamics expand and buffer the responses of complex systems: The diverse plant actin gene family. *Plant Cell* 11, 995–1005. doi: 10.2307/3870793

Michelot, A., Guérin, C., Huang, S. J., Ingouff, M., Richard, S., Rodiuc, N., et al. (2005). The formin homology 1 domain modulates the actin nucleation and bundling activity of Arabidopsis FORMIN1. *Plant Cell* 17, 2296–2313. doi: 10.1111/j.1465-7295.2008.00159.x

Miller, D. D., Ruijter, N. C., Bisseling, T., and Emons, A. M. (1999). The role of actin in root hair morphogenesis: studies with lipochito-oligosaccharide as a growth stimulator and cytochalasin as an actin perturbing drug. *Plant J.* 17, 141–154. doi: 10.1046/j.1365-313X.1999.00358.x

Morin, M., Bryanm, K. E., Mayo, F., Goodyear, R., Mencia, A., Modamino, S., et al. (2009). *In vivo* and *in vitro* effects of two novel gamma-actin (*ACTG1*) mutations that cause DFNA20/26 hearing impairment. *Hum. Mol. Genet.* 18, 3075–3089. doi: 10.1093/hmg/ddp249

Nishimura, T., Yokota., E., Wada, T., Shimmen, T., and Okada, K. (2003). An Arabidopsis *ACT2* dominant-negative mutation, which disturbs F-actin polymerization, reveals its distinctive function in root development. *Plant Cell Physiol.* 44, 1131–1140. doi: 10.1093/pcp/pcg158

Paterson, A. H., Wendel, J. F., Gundlach, H., Guo, H., Jenkins, J., Jin, D. C., et al. (2012). Repeated polyploidization of *Gossypium* genomes and the evolution of spinnable cotton fibres. *Nature* 492, 423–427. doi: 10.1038/nature11798

Pei, W. K., Du, F., Zhang, Y., He, T., and Ren, H. Y. (2012). Control of the actin cytoskeleton in root hair development. *Plant Sci.* 187, 10–18. doi: 10.1016/j.plantsci.2012.01.008

Pierick, A. R., Mckane, M., Wen, K. K., and Bartlett, H. L. (2014). Aip1p dynamics are altered by the R256H mutation in actin. *Jove-J Vis Exp.* 89, e51551–e51557. doi: 10.3791/51551

Pollard, T. D., and Cooper, J. A. (1986). Actin and actin-binding proteins. A critical evaluation of mechanisms and functions. *Annu. Rev. Biochem.* 55, 987–1035. doi: 10.1146/annurev.bi.55.070186.005011

Ramachandran, S., Christensen, H. E. M., Ishimaru, Y., Dong, C. H., Wen, C. M., Cleary, A. L., et al. (2000). Profilin plays a role in cell elongation, cell shape maintenance, and flowering in Arabidopsis. *Plant Physiol.* 124, 1637–1647. doi: 10.1104/pp.124.4.1637

Ringli, C., Baumberger, N., Diet, A., Frey, A., and Keller, B. (2002). ACTIN2 is essential for bulge site selection and tip growth during root hair development of Arabidopsis. *Plant Physiol.* 129, 1464–1472. doi: 10.1002/pssb.2221880214

Rong, J. K., Pierce, G. J., Waghmare, V. N., Rogers, C., Desai, A., Chee, P. W., et al. (2005). Genetic mapping and comparative analysis of seven mutants related to seed fiber development in cotton. *Theor. Appl. Genet.* 111, 1137–1146. doi: 10.1007/s00122-005-0041-0

Schubert, A. M., Benedict, C. R., Berlin, J. D., and Kohel, R. J. (1973). Cotton fiber development-kinetics of cell elongation and secondary wall thickening. *Crop Sci.* 13, 704–709. doi: 10.2135/cropsci1973.0011183X001300060035x

Seagull, R. W. (1990). The effects of microtubule and microfilament disrupting agents on cytoskeletal arrays and wall deposition in developing cotton fibers. *Protoplasma* 159, 44–59. doi: 10.1007/bf01326634

Senthilkumar, M., and Mysore, K. S. (2011). Caveat of RNAi in plants: The off-target effect. *Methods Mol. Biol.* 744, 13–25. doi: 10.1007/978-1-61779-123-9_2

Si, Z., Liu, H., Zhu, J. K., Chen, J. D., Wang, Q., Fang, L., et al. (2018). Mutation of *SELF-PRUNING* homologs in cotton promotes short-branching plant architecture. *J. Exp. Bot.* 69, 2543–2553. doi: 10.1093/jxb/ery093

Šlajcherová, K., Fišerová, J., Fischer, L., and Schwarzerová, K. (2012). Multiple actin isotypes in plants: diverse genes for diverse roles?. *Front. Plant Sci.* 3, 226–234. doi: 10.3389/fpls.2012.00226

Staiger, C. J., Baluška, F., Volkmann, D., and Barlow, P. W. (2000). *Actin: a dynamic framework for multiple plant cell functions.* Dordrecht, The Netherlands: Kluwer Academic Publishers. doi: 10.1007/978-94-015-9460-8

Szymanski, D. B., Marks, M. D., and Wick, S. M. (1999). Organized F-actin is essential for normal trichome morphogenesis in Arabidopsis. *Plant Cell* 11, 2331–2347. doi: 10.2307/3870959

Tang, J. Y., Zhu, X. D., Wang, Y. Q., Liu, L. C., Xu, B., Li, F., et al. (2011). Semi-dominant mutations in the CC-NB-LRR-type *R* gene, *NLS1*, lead to constitutive activation of defense responses in rice. *Plant J.* 66, 996–1007. doi: 10.1111/j.1365-313X.2011.04557.x

Teal, D. J., and Dawson, J. F. (2007). Yeast actin with a subdomain 4 mutation (A204C) exhibits increased pointed-end critical concentration. *Biochem. Cell Biol.* 85, 319–325. doi: 10.1016/S0378-7796(03)00022-1

Thyssen, G. N., Fang, D. D., Turley, R. B., Florane, C., Li, P., and Naoumkina, M. (2015). Mapping-by-sequencing of Ligon-lintless-1 (Li$_1$) reveals a cluster of neighboring genes with correlated expression in developing fibers of Upland cotton (*Gossypium hirsutum* L.). *Theor. Appl. Genet.* 128, 1703–1712. doi: 10.1007/s00122-015-2539-4

Thyssen, G. N., Fang, D. D., Turley, R. B., Florane, C. B., Li, P., Mattison, C. P., et al. (2017). A Gly65Val substitution in an actin, GhACT_LI1, disrupts cell polarity and F-actin organization resulting in dwarf, lintless cotton plants. *Plant J.* 90, 111–121. doi: 10.1111/tpj.13477

Trapnell, C., Roberts, A., Goff, L., Pertea, G., Kim, D., Kelley, D. R., et al. (2012). Differential gene and transcript expression analysis of RNA-seq experiments with TopHat and Cufflinks. *Nat. Protoc.* 7, 562–578. doi: 10.1038/nprot.2012.016

Wang, H. Y., Yu, Y., Chen, Z. L., and Xia, G. X. (2005). Functional characterization of *Gossypium hirsutum* profilin 1 gene (*GhPFN1*) in tobacco suspension cells: Characterization of *in vivo* functions of a cotton profilin gene. *Planta* 222, 594–603. doi: 10.1007/s00425-005-0005-2

Wang, X. H., Teng, Y., Wang, Q. L., Li, X. J., Sheng, X. Y., Zheng, M. Z., et al. (2006). Imaging of dynamic secretory vesicles in living pollen tubes of *Picea meyeri* using evanescent wave microscopy. *Plant Physiol.* 141, 1591–1603. doi: 10.1104/pp.106.080168

Wang, H. Y., Wang, J., Gao, P., Jiao, G. L., Zhao, P. M., Li, Y., et al. (2009). Down-regulation of *GhADF1* gene expression affects cotton fibre properties. *Plant Biotechnol. J.* 7, 13–23. doi: 10.1111/j.1467-7652.2008.00367.x

Wang, J., Wang, H. Y., Zhao, P. M., Han, L. B., Jiao, G. L., Zheng, Y. Y., et al. (2010). Overexpression of a profilin (GhPFN2) promotes the progression of developmental phases in cotton fibers. *Plant Cell Physiol.* 51, 1276–1290. doi: 10.1093/pcp/pcq086

Wu, S. J., Wang, H. H., Li, F. F., Chen, T. Z., Zhang, J., Jiang, Y. J., et al. (2008). Enhanced *Agrobacterium*-mediated transformation of embryogenic calli of upland cotton *via* efficient selection and timely subculture of somatic embryos. *Plant Mol. Biol. Rep.* 26, 174–185. doi: 10.1007/s11105-008-0032-9

Wu, S. Y., Xie, Y. R., Zhang, J. J., Ren, Y. L., Zhang, X., Wang, J. L., et al. (2015). *VLN2* regulates plant architecture by affecting microfilament dynamics and polar auxin transport in rice. *Plant Cell* 27, 2829–2845. doi: 10.1105/tpc.15.00581

Xu, P., Zhang, Y. J., Kang, L., Roossinck, M. J., and Mysore, K. S. (2006). Computational estimation and experimental verification of off-target silencing during posttranscriptional gene silencing in plants. *Plant Physiol.* 142, 429–440. doi: 10.1104/pp.106.083295

Yang, W. B., Ren, S. L., Zhang, X. M., Gao, M. J., Ye, S. H., Qi, C. B., et al. (2011). *BENT UPPERMOST INTERNODE1* encodes the class II formin FH5 crucial for actin organization and rice development. *Plant Cell* 23, 661–680. doi: 10.1105/tpc.110.081802

Zhai, S. N., Li, G. Y., Sun, Y. W., Song, J. M., Liu, J. H., Song, G. Q., et al. (2016). Genetic analysis of phytoene synthase 1 (*Psy1*) gene function and regulation in common wheat. *BMC Plant Biol.* 16, 228–240. doi: 10.1186/s12870-016-0916-z

Zhang, Z., Zhang, Y., Tan, H. X., Wang, Y., Li, G., Liang, W. Q., et al. (2011). *RICE MORPHOLOGY DETERMINANT* encodes the type II formin FH5 and regulates rice morphogenesis. *Plant Cell* 23, 681–700. doi: 10.1105/tpc.110.081349

Zhang, T. Z., Hu, Y., Jiang, W. K., Fang, L., Guan, X. Y., Chen, J. D. et al.(2015). Sequencing of allotetraploid cotton (*Gossypium hirsutum* L. acc. TM-1) provides a resource for fiber improvement. *Nat. Biotechnol.* 2015 33, 531–537. doi: 10.1038/nbt.3207

Zhang, M., Han, L. B., Wang, W. Y., Wu, S. J., Jiao, G. L., Su, L., et al. (2017). Overexpression of *GhFIM2* propels cotton fiber development by enhancing actin bundle formation. *J. Integer. Plant Biol.* 59, 531–534. doi: 10.1111/jipb.12552

Zhao, P. M., Wang, L. L., Han, L. B., Wang, J., Yao, Y., Wang, H. Y., et al. (2010). Proteomic identification of differentially expressed proteins in the Ligon lintless mutant of upland cotton (*Gossypium hirsutum* L.). *J. Proteome Res.* 9, 1076–1087. doi: 10.1021/pr900975t